LHCb Alignment Strategy

W. Baldini

Istituto Nazionale di Fisica Nucleare, Ferrara (INFN)

J. Blouw

Physikalisches Institut, Heidelberg

S. Blusk

Syracuse University

N. Gilardi

University of Edinburgh

O. Deschamps

Université Blaise Pascal de Clermont-Ferrand II

F. Maciuc

Max-Planck-Institut für Kernphysik (MPI)

J. Nardulli

NIKHEF

A. Papanestis

Rutherford Appleton Laboratory

C. Parkes, S. Viret

Glasgow University

M. Needham

CERN

J. van Tilburg

Universität Zürich

S. Vecchi

Istituto Nazionale di Fisica Nucleare, Bologna (INFN)

K. Vervink

Ecole Polytechnique Fédérale de Lausanne (LPHE)

LHCb Experiment

Abstract

In this note, we review the alignment strategy for the LHCb detector. We discuss the internal alignment stategy for each subdetector and the alignment of each of the subdetectors relative to one another.

Document Status Sheet

1. Document Title: LHCb Alignment Strategy			
2. Document Reference Number: LHCb-2006-035			
3. Issue	4. Revision	5. Date	6. Reason for change
Draft	1	June 19, 2006	First version

Contents

List of Figures

List of Tables

LHCb Alignment Strategy
LHCb Experiment
1 Introduction

Ref: *LHCb-2006-035*
Issue: *1*
Date: *June 19, 2006*

1   Introduction

The LHCb experiment is designed to search for new physics, primarily through the decays of mesons containing a bottom quark. The design takes advantage of (a) the correlated forward production of b and $\bar{b}$ quarks, (b) their long lifetime, leading to a decay point which is significantly displaced from the interaction point, and (c) the higher transverse momentum of particles in $b\bar{b}$ events as compared to minimum bias events, in order to trigger on and record a large sample of events containing B mesons.

A diagram of the LHCb detector is shown in Fig. 1. The detector consists of several subdetectors for charged particle tracking, a pair of RICH detectors for particle identification, an electromagnetic (ECAL) and hadronic calorimeter (HCAL) for triggering on high transverse momentum and reconstruction of EM showers, and a muon system for triggering on events with (di)muons and identifying muons in the event reconstruction. From left to right, the tracking system consists of a silicon strip detector, called the Vertex Locator (VELO) [1, 2], which enables precise charged particle tracking near the interaction point and allows for the reconstruction of the interaction vertices and decays of long-lived hadrons. About 2.5 meters downstream of the VELO is another set of silicon planes, referred to as the Trigger Tracker (TT) [1, 3]. It serves to provide a rough estimate of the momentum which is used in the trigger to select high transverse momentum particles, as well as aid in charged particle reconstruction. The third pair of subdetectors, situated ∼7.5-9.5 meters downstream of the VELO, are three tracking stations, each comprised of a silicon-strip based Inner Tracker (IT) [1, 4] and a straw-tube based Outer Tracker [1, 5]. Collectively, they are referred to as the T-Stations. They provide hit information for charged particles downstream of the large dipole analysis magnet [6], enabling the reconstruction of the charged particles and measurement of their momenta. Charged particle identification is provided by two Ring Imaging Cherenkov Detectors (RICH1 and RICH2) [1, 7]. Both systems focus and detect Cherenkov photons onto arrays of hybrid photo-diodes (HPD) using two arrays of mirrors. The first set of mirrors are spherical which provide focusing and the second set is flat and redirects the photons onto the HPD array which is outside the detector acceptance. The ECAL and HCAL [8] provide for a fast Level 0 trigger based on transverse energy deposition. Offline, the ECAL is used to identify electrons and reconstruct π^0 decays. The muon system [9] provides a fast Level 0 trigger to select events containing high transverse momentum muons and is used to identify muons in the event reconstruction. All of these subdetectors are used in some way in the three-level trigger system [10] designed to select a highly enriched sample of events containing b (and c)-hadrons.

The overall alignment of the LHCb detector will influence the final physics performance of the detector. Poor alignments can lead to worse mass resolution, for example, or even lead to systematic biases which can plague sensitive asymmetry measurements. It is therefore of utmost importance to ensure that all detector components are brought into relative alignment to a level which has negligible impact on physical observables.

LHCb presents some technical details which differ from other LHC experiments. In particular, prior to the LHC establishing stable beams, the VELO is retracted by ∼3 cm (open position), and is step-wise brought into its nominal position only after stable beam is established. The nominal location places the first R strip of the VELO at a radius of about 8.16 mm from the interaction point. The motion controller of the VELO provides a readback of the actual position of the VELO with respect to the fully open position to an accuracy of 10 μm. Since we expect to align the T-Stations to the VELO and the rest of the LHCb subdetectors to the tracking system, the 10 μm precision in the absolute position of the VELO implies a 10 μm uncertainty on the absolute position of the LHCb detector. The internal software alignment precision of the VELO will be significantly better than this ($O(2\,\mu\text{m})$). The alignment of the T-Stations with respect to the VELO is expected to have a precision of order 20 μm, which is about 50 times better than intrinsic resolution obtained when matching VELO and T-Station track segments, and therefore should have minimal impact on physical obsevables. Only the relative alignment between detector elements and subdetectors affects physical observables, such as invariant masses, and we expect to achieve a precision on them such that there is negligible degradation in the physical observables.

A second technical point related to alignment is that the LHCb magnet will not be kept at full field while the LHC is stacking the accelerator with protons. After each fill, the field will be reduced to some intermediate value, and its ramp up to full field will be coordinated and controlled by the LHC beam controls. As the LHCb magnet is brought up to full field, it is conceivable that sub-detectors

LHCb Alignment Strategy
LHCb Experiment
1   Introduction

Ref: *LHCb-2006-035*
Issue: *1*
Date: *June 19, 2006*
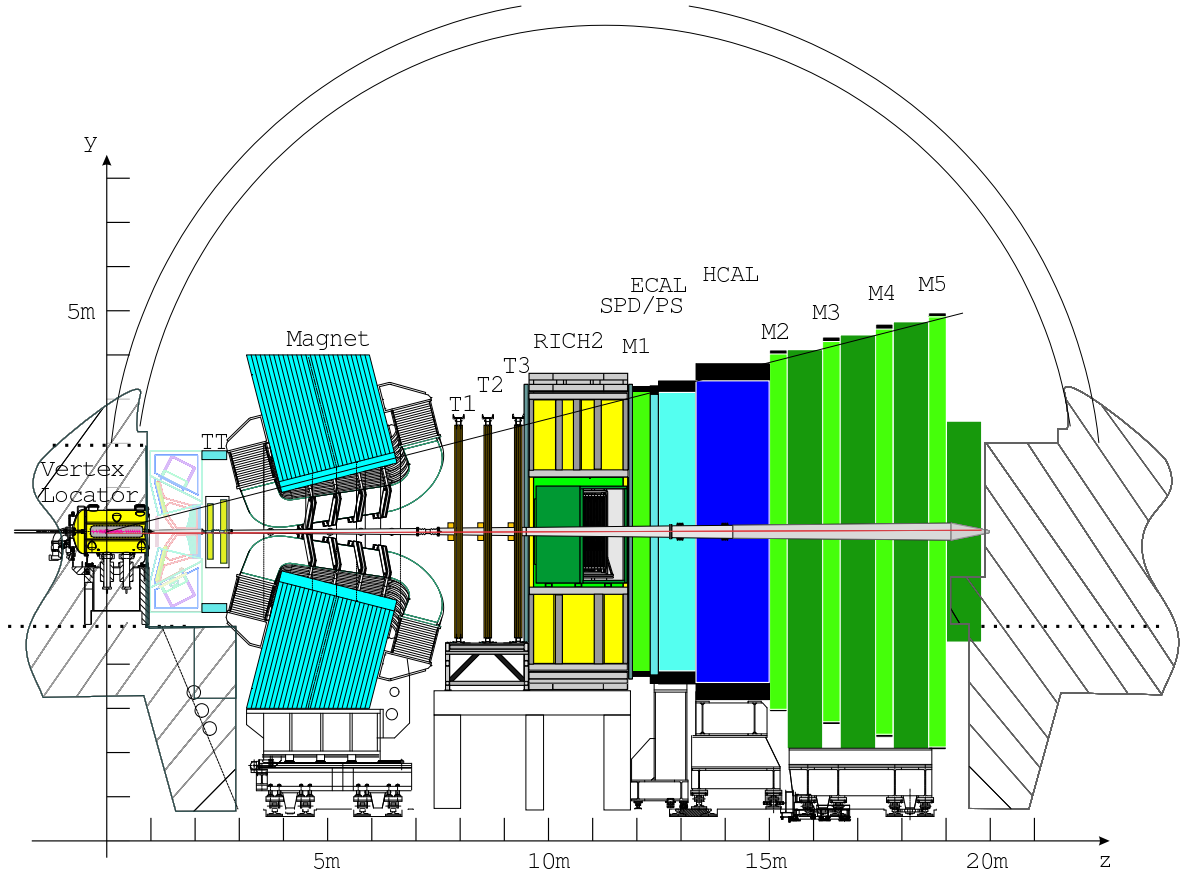
Figure 1 Layout of the LHCb detector as described in the text.

LHCb Alignment Strategy
LHCb Experiment
1   Introduction

Ref: *LHCb-2006-035*
Issue: *1*
Date: *June 19, 2006*

close to the magnet will shift slightly. Both TT and RICH1 are particularly close to the magnet, and may deflect as the field is brought up to its nominal value. It is not known at this time how much the chambers will shift, if at all, and whether or not they will shift by the same amount each time the field is cycled. LHCb is also considering regular flipping of the polarity of the B field to possibly better understand detector-induced asymmetries. The alignment shifts for the opposite polarities may not be equal and opposite.

Since the higher level triggers of LHCb trigger rely on tracking and particle identification, it is important that the entire detector, particularly the tracking system and RICH detectors, is in relative alignment prior to taking physics quality data. The two aforementioned effects may require a different set of alignment constants for each fill of the LHC that take into account these small global shifts.

Typically, tracking detectors are aligned by requiring that the hits produced by charged particles lie along a trajectory which is assumed to be known. If no magnetic field is present, the trajectory is linear in a Cartesian coordinate system. However, if a magnetic field is present, the trajectory is curved, and the predicted position of the particle at any location will depend on how well the momentum and the magnetic field, $B(x, y, z)$ are known. It has been observed by several forward spectrometer experiments that the geometrical alignment of the tracking system can be obscured when using only data with the magnetic field present [11]. This arises due to either an imperfect understanding or modeling of the field and this bias will be propagated to and hidden in the geometrical alignment constants. To remove this bias, the tracking system should first be fully aligned with magnetic field off data, and then adjusted once the field is brought up to its nominal value. In the latter case, most of the internal degrees of freedom are generally fixed using the magnet off data, and only the global degrees of freedom of each detector plane (three translations and three rotations) need to be determined with magnet on data. With much fewer (global) alignment parameters to be determined, the demands on alignment algorithms are significantly reduced, and we expect that the global alignment parameters can be reliably extracted even with magnet on data.

The first step of the alignment procedure is to determine the internal alignment constants of each detection plane. For LHCb, the VELO and the T-Stations are in the fringe field of the LHCb magnet, and thus both have a non-zero field integral, $\int \vec{B} \cdot \vec{dl}$. The hits produced by charged particles can be used to independently reconstruct segments of charged particles in the VELO and the T-Stations. Using these charged particle segments, the VELO and T-Stations can be internally aligned. In this step, all geometrical offsets (x, y, z translations and 3 Euler angles) of each detector element are determined, as well as possible out-of-plane distortions. As most subdetectors are split along the Y-axis to accommodate the beam pipe, this amounts to a doubling of these internal alignment parameters. All of these internal alignment constants can be determined precisely with a sufficient size data sample.

The aim of this document is to describe the LHCb alignment strategy. The alignment of the LHCb detector can be separated into several general steps:

1. Internal alignment of the Vertex Locator (VELO) halves and the VELO halves to one another (Section 2)

2. Internal alignment of the IT, OT and the IT-to-OT (Section 3)

3. Relative alignment of VELO to IT/OT (Section 4)

4. Alignment of the Trigger Tracker with tracks formed using VELO and IT/OT hits (Section 3)

5. Alignment of the RICH using fully aligned tracking system (Section 5)

6. Alignment of ECAL and HCAL using fully aligned tracking system (Section 6)

7. Alignment of the MUON system using fully aligned tracking system (Section 7)

8. Coordinates in the LHCb global frame (Section 8)

9. Storage and Retrieval of Alignment Constants (Section 9)

LHCb Alignment Strategy
LHCb Experiment
1   Introduction

Ref: *LHCb-2006-035*
Issue: *1*
Date: *June 19, 2006*

These steps are first carried out using magnet off data. Steps 1 and 2 can be carried out in parallel, followed by step 3 and then step 4. Steps 5-7 can also be carried out in parallel if advantageous. We direct the reader to the relevant sections, as indicated in parentheses, for the relevant discussion. For each section, we describe what has been done to address the alignment issues, and discuss future plans to finish the task.

Throughout this document, where appropriate, we use the LHCb coordinate system. The origin of the LHCb coordinate system will be fixed and is nominally given by the center of the expected interaction region. The z-axis points along the beam direction from the VELO toward the MUON system, the y axis points upward, and the x-axis points toward the outside of the LHC ring, thus creating a right-handed coordinate system. In placing the sub-detectors, those upstream of the LHCb magnet follow the angle of the beam, whose direction is inclined at $+3.601$ mrad with respect to a z axis which is at $90°$ with respect to the gravitational y axis. The z axis of the detectors downstream of the LHCb magnet are not tilted, and thus their y axes are aligned with the gravitational direction. The definitions of the various coordinate systems are described in Ref. [13].

LHCb Alignment Strategy
LHCb Experiment
2   VELO Alignment

Ref: *LHCb-2006-035*
Issue: *1*
Date: *June 19, 2006*

2   VELO Alignment

2.1   Introduction

The VELO software alignment algorithm must be able to align the modules within each of the two VELO-half boxes and also to align the two half-boxes themselves within the VELO reference frame. The two VELO half boxes will be retracted and reinserted between each LHC fill. However, the alignment with tracks cannot give us information about the absolute box positions in the LHCb frame. This requires a global alignment of the full VELO system with respect to the other sub-detectors.

The VELO alignment procedure naturally divides into two distinct parts:

1. An internal alignment of the modules within each VELO-half box using the residuals of hits on reconstructed tracks.

2. A relative alignment of the two boxes with respect to each other using primary vertices, module overlaps, and tracks crossing both halves.

In this approach, the equations which describe the trajectories of particles are expressed as a linear combination of the local (track-dependent) parameters and the global (alignment) parameters. A χ^2 can then be written, which contains both the track and alignment parameters, each of which are obtained through minimization of this χ^2 function. By matrix inversion, one then obtains in a single step the alignment and tracks parameters.

2.2   Internal Alignment

An algorithm to perform the first alignment stage has been proposed and described in Ref. [14] and is briefly summarized in this section. The chosen technique is a non-iterative method using the matrix inversion program *Millepede* [15], which has been integrated into the LHCb software and tested. In this approach, the equations which describe the trajectories of particles are expressed as a linear combination of the local (track-dependent) parameters and the global (alignment) parameters. A χ^2 can then be written, which contains both the track and alignment parameters, each of which are obtained through minimization of this χ^2 function. The resulting matrix is formally of dimension $N_{\mathrm{global}} + N_{\mathrm{track}} \times N_{\mathrm{local}}$, where N_{global} and N_{local} are the number of global alignment parameters (such as x, y, z offsets, and corresponding rotations of each plane), N_{local} are the local track parameters, and N_{track} are the number of tracks used in the χ^2 fit. The inversion of such large matrices is not computationally practical. Millepede handles the matrix inversion by reducing the matrix to block diagonal form, where one of the blocks is of dimension $N_{\mathrm{global}} \times N_{\mathrm{global}}$ and contains only the global alignment parameters. Therefore, one only needs to invert a matrix of dimension $N_{\mathrm{global}} \times N_{\mathrm{global}}$ to obtain in one step the global alignment parameters.

The results of the internal alignment algorithm have been evaluated using simulated events and are reported in this section. Two-hundred samples of 2000 minimum bias Monte Carlo (MC) events have been produced and propagated through LHCb simulation packages. Each sample has a different set of alignment constants, which are introduced into the LHCb geometry using the recently developed LHCb Geometry Framework described in Ref. [16].

The misalignment values have been randomly chosen within a Gaussian distribution centered on 0 and with the resolution σ_{scale}. The different scales are summarized in Table 1. Module rotations and translations have been considered. In addition, the constraints equations on the box translations have been tested by introducing box misalignments. It should be noted that the VELO measures R and ϕ, which are transformed to x, y coordinates for use in Millepede.

2.2.1   *Effect on misalignments*

The robustness of the method is demonstrated (using the 200 samples) in Figs. 2 for x and y translations, and in Fig 3 for z rotations. The few outlying points in Fig. 3 originate from stations close to the

Table 1 Misalignment scales, approximately corresponding to those expected from mechanical tolerances, which were used to generate the simulation samples. Δ_α, Δ_β, Δ_γ describe small rotations around the x, y, and z axes, respectively.

Component	Degree of freedom	σ_{scale}
Module	Δ_x, Δ_y, Δ_z	$30\ \mu m$
Module	Δ_α, Δ_β, Δ_γ	$2\ mrad$

interaction point (mainly stations 7 and 8). It is anticipated that these effects will disappear when using a sample of tracks that has a higher population on the outer part of the sensor (such as beam halo tracks). Apart from that, all the relevant misalignments are well corrected, even those with a relatively large scale.

A fit of the corrected alignment constants is shown on Fig. 4. Translational misalignments are corrected to a 2.8 μm accuracy (better than the best possible VELO resolution), whereas a 0.4 mrad precision is obtained for rotation around the z axis. The resolution for the rotations is not as good as for the translations but is already very acceptable as it is at the level of $1/6^{th}$ of a ϕ outer strip.

2.2.2   *Effect on residuals*

After the alignment procedure the quality of the track parameters should be improved. One way to check this is to compare the track residuals before and after the alignment procedure.

One has:

$$\begin{cases} \epsilon_x & = & x_{measured} - x_{track} \\ \epsilon_y & = & y_{measured} - y_{track} \end{cases} . \tag{1}$$

Since the VELO has an (R, ϕ) geometry, we will present residuals values in R and ϕ directions:

$$\begin{cases} \epsilon_R & = & \sqrt{(x_{measured} + \epsilon_x)^2 + (y_{measured} + \epsilon_y)^2} - \sqrt{x_{measured}^2 + y_{measured}^2} \\ \epsilon_\phi & = & atan(\frac{y_{measured} + \epsilon_y}{x_{measured} + \epsilon_x}) - atan(\frac{y_{measured}}{x_{measured}}) \end{cases} . \tag{2}$$

The x and y residuals before and after alignment are presented in Fig. 5. Residual values as a function of R and ϕ are shown in Fig. 6 and 7, We see that in all cases the mean value of the residuals is centered on zero after the alignment procedure and that the root-mean square (RMS) of the distribution is also slightly improved.

2.3   Box Alignment

The second step of the alignment procedure is to position the two RF boxes into the VELO reference frame. To perform the relative box alignment we need to identify constraints which establish a relationship between the two VELO half-boxes. We have considered two candidates: using the fact that physics tracks are produced from a common primary vertex; and considering tracks which pass trough the overlap region between the modules in the left and right VELO half-boxes. This work will be the subject of a future note.

2.3.1   *Primary vertices*

Previously we performed an alignment using the residuals of hits to tracks to obtain an internal alignment of the modules in each VELO half. The result of this procedure is that each VELO half is internally aligned. The next step of the VELO alignment is to use the interaction point, which is obviously common to all (primary) tracks, to align the two halves with respect to one another. Implementing a fit to the primary vertex in a Millepede-based formalism is relatively simple and is described in

Ref. [14]. In short, the relative alignment of the two VELO halves can be obtained by constraining the two halves to yield the same primary vertex location, while allowing for relative translations and rotations of the two VELO halves with respect to one another.

Preliminary tests performed with translations to the VELO halves have shown encouraging results (see Fig. 8), as a 10 μm precision has been obtained during robustness tests. Rotations (or tilts) of each VELO half are more difficult to unfold using only primary vertices, and a method based on overlapping tracks is currently under investigation.

2.3.2   Overlaps

The overlap region of the LHCb VELO left and right hand modules (shown in Fig. 9) are relatively small: this is mainly due to the 'dog-leg' shape of the ϕ sensor. The main consequence of this geometry is that it is almost impossible to have a 'perfect' overlap, *i.e.* two pairs of (r, ϕ) clusters in two adjacent modules from opposite halves of the VELO. However, it is not uncommon to have a track which contains one or more (r, ϕ) clusters pairs in both halves of the VELO.

Such a situation should fit nicely with our alignment procedure, as we only require (x, y) space-points for the alignment algorithm. However, these tracks are in an area containing a significant amount of material (RF foils) where secondary interactions and large multiple scattering are expected. Hence, the pattern recognition code will have to be optimized to minimize the selection of incorrect hits as these can lead to a bias in the alignment.

LHCb Alignment Strategy
LHCb Experiment
2   VELO Alignment

Ref: *LHCb-2006-035*
Issue: *1*
Date: *June 19, 2006*
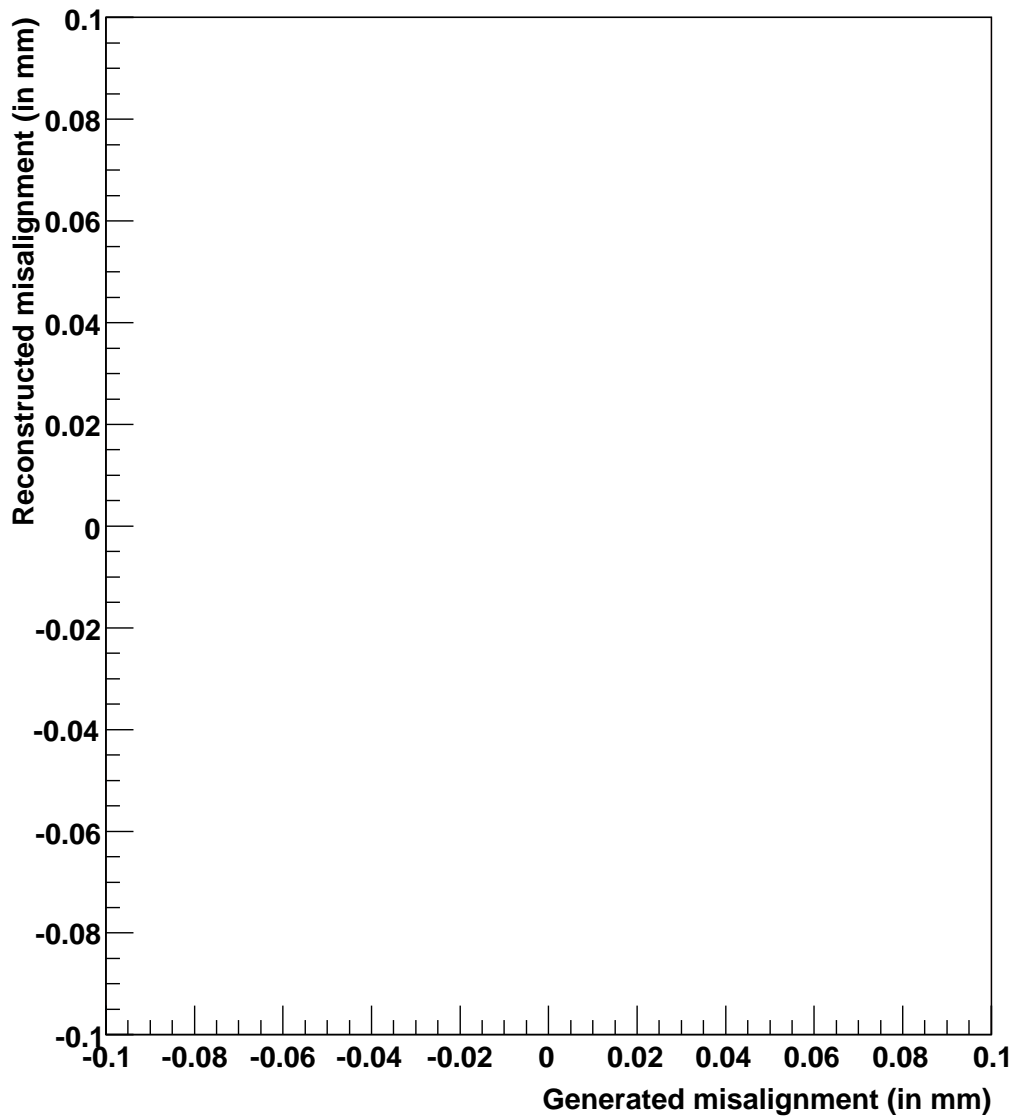
Figure 2 Internal alignment robustness tests: results for the translations, for dx and dy misalignments (200 sets of misalignments).

LHCb Alignment Strategy
LHCb Experiment
2   VELO Alignment

Ref: *LHCb-2006-035*
Issue: *1*
Date: *June 19, 2006*
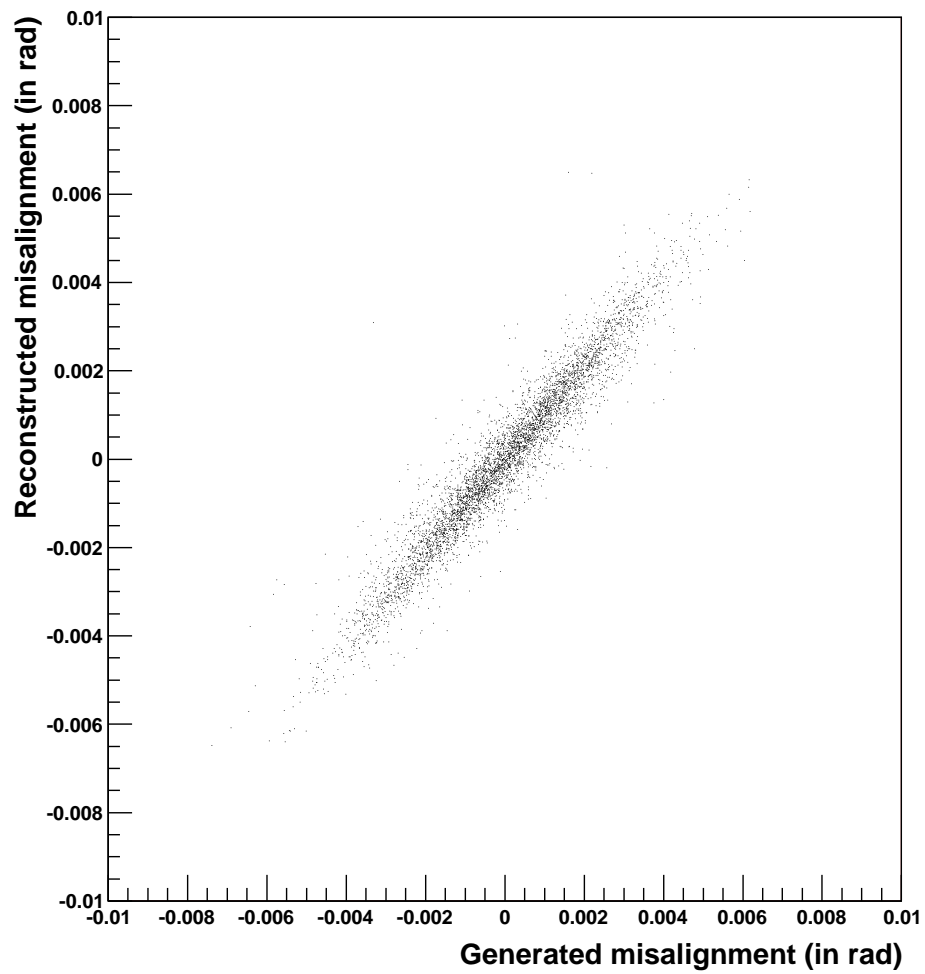
Figure 3 Internal alignment robustness tests: results for the rotations, for $d\gamma$ misalignments (200 sets of misalignments).

LHCb Alignment Strategy
LHCb Experiment
2   VELO Alignment

Ref: *LHCb-2006-035*
Issue: *1*
Date: *June 19, 2006*
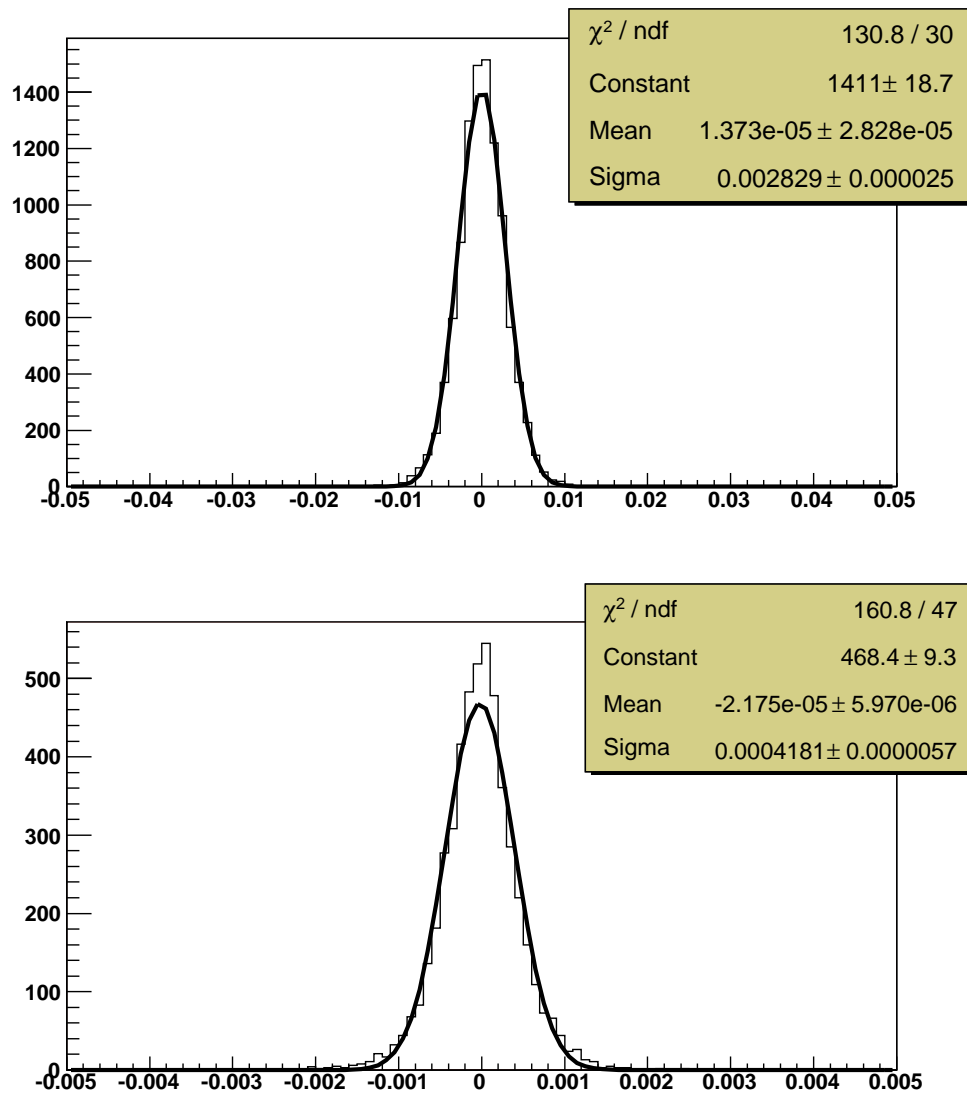
Figure 4 Internal alignment robustness tests: resolution on the corrected misalignment constants (200 sets of misalignments). Top plot shows the result for the x and y translations (in mm), bottom plot shows the result for z rotation (in rad).

LHCb Alignment Strategy
LHCb Experiment
2   VELO Alignment

Ref: *LHCb-2006-035*
Issue: *1*
Date: *June 19, 2006*
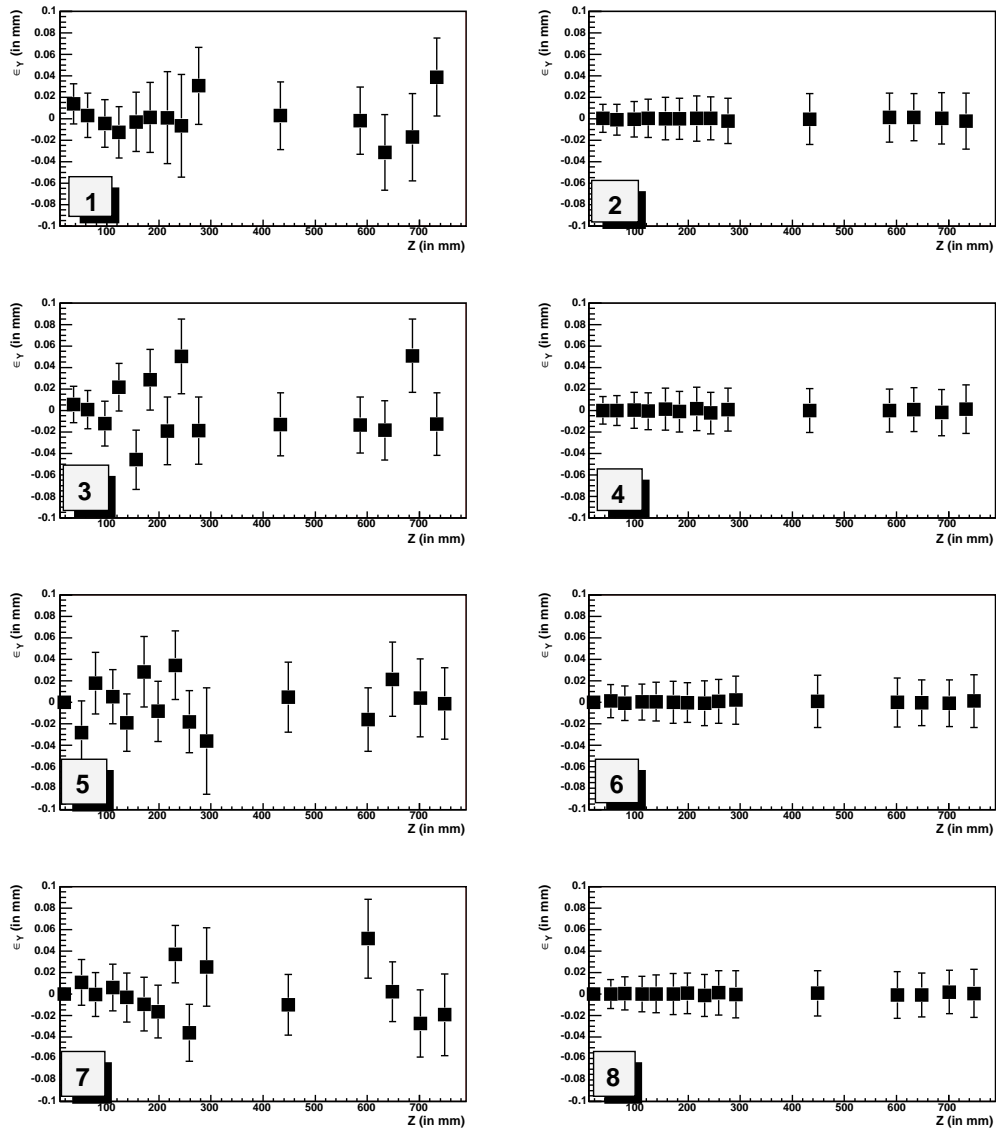
Figure 5 Track residuals summary plot, as a function of z position of the modules. Left plots are before internal alignment, right plots after. The plots 1,2 show the x residuals for the left half-box. The plots 3,4 show the y residuals for the left half-box. Plots 5,6,7 and 8 show the same results for the right half-box. Error bars correspond to the RMS of the residual distributions.

LHCb Alignment Strategy
LHCb Experiment
2   VELO Alignment

Ref: *LHCb-2006-035*
Issue: *1*
Date: *June 19, 2006*
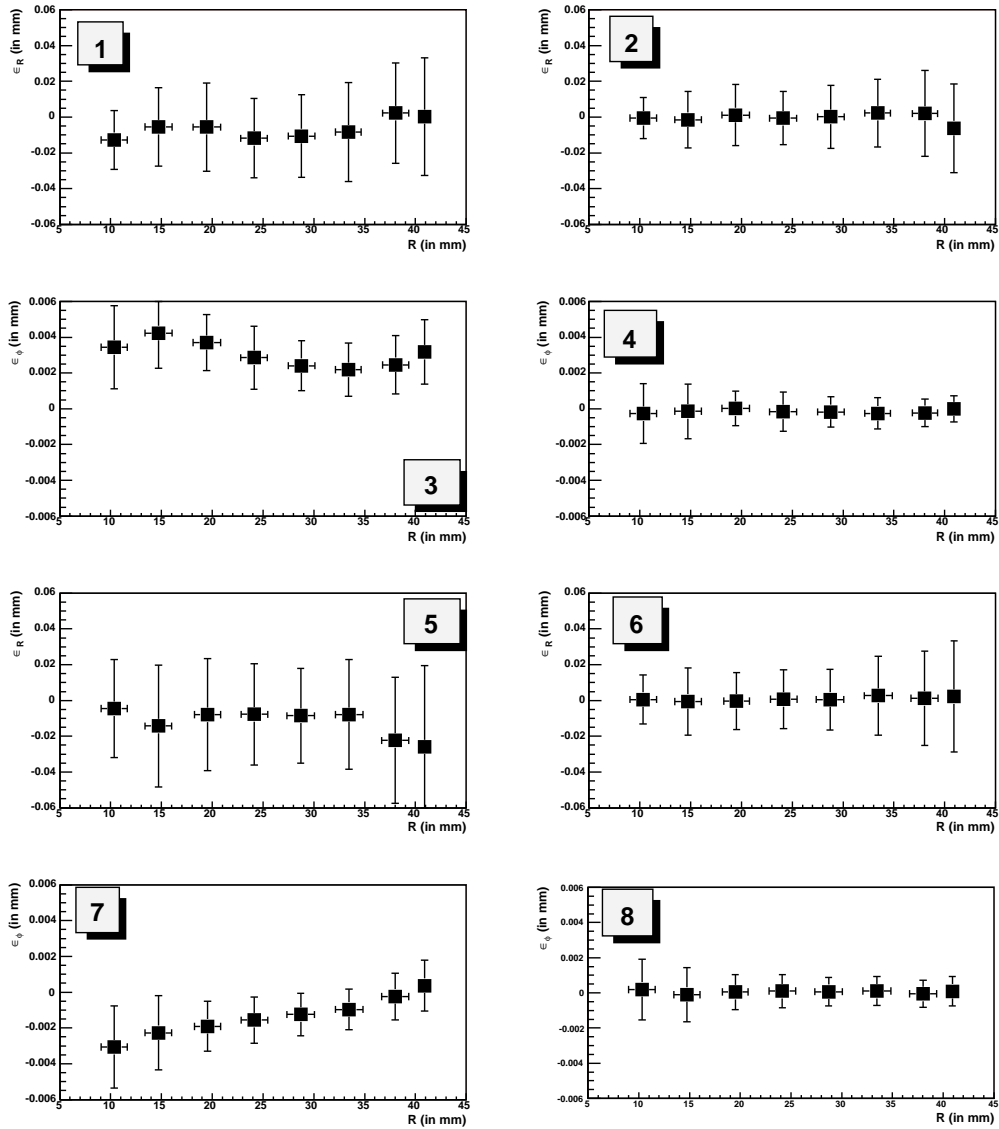
Figure 6 Track residuals as a function of R, for one particular station (station 14) and one particular set of misalignments. Left plots are before internal alignment, and right plots are after. They show the left box R and ϕ residuals (resp. 1,2 and 3,4), and right box R and ϕ residuals (resp. 5,6 and 7,8). Error bars correspond to the RMS of the residual distributions.

LHCb Alignment Strategy
LHCb Experiment
2   VELO Alignment

Ref: *LHCb-2006-035*
Issue: *1*
Date: *June 19, 2006*
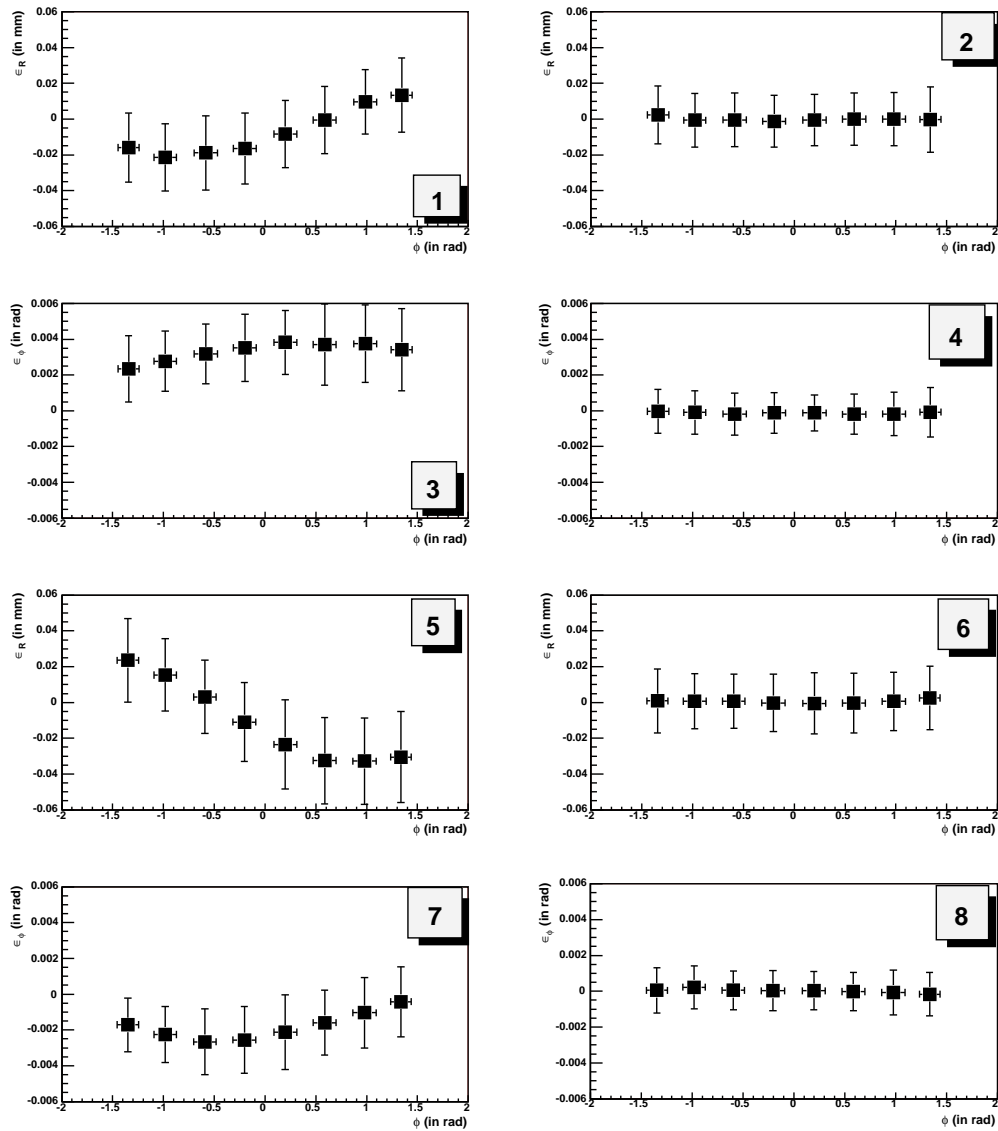
Figure 7 Track residuals as a function of ϕ (same run and same set of misalignment than previous figure). Left plots are before internal alignment, and right plots after. The plots show the left box R and ϕ residuals (resp. 1,2 and 3,4), and right box R and ϕ residuals (resp. 5,6 and 7,8). Error bars correspond to the RMS of the residual distributions.

LHCb Alignment Strategy
LHCb Experiment
2   VELO Alignment

Ref: *LHCb-2006-035*
Issue: *1*
Date: *June 19, 2006*
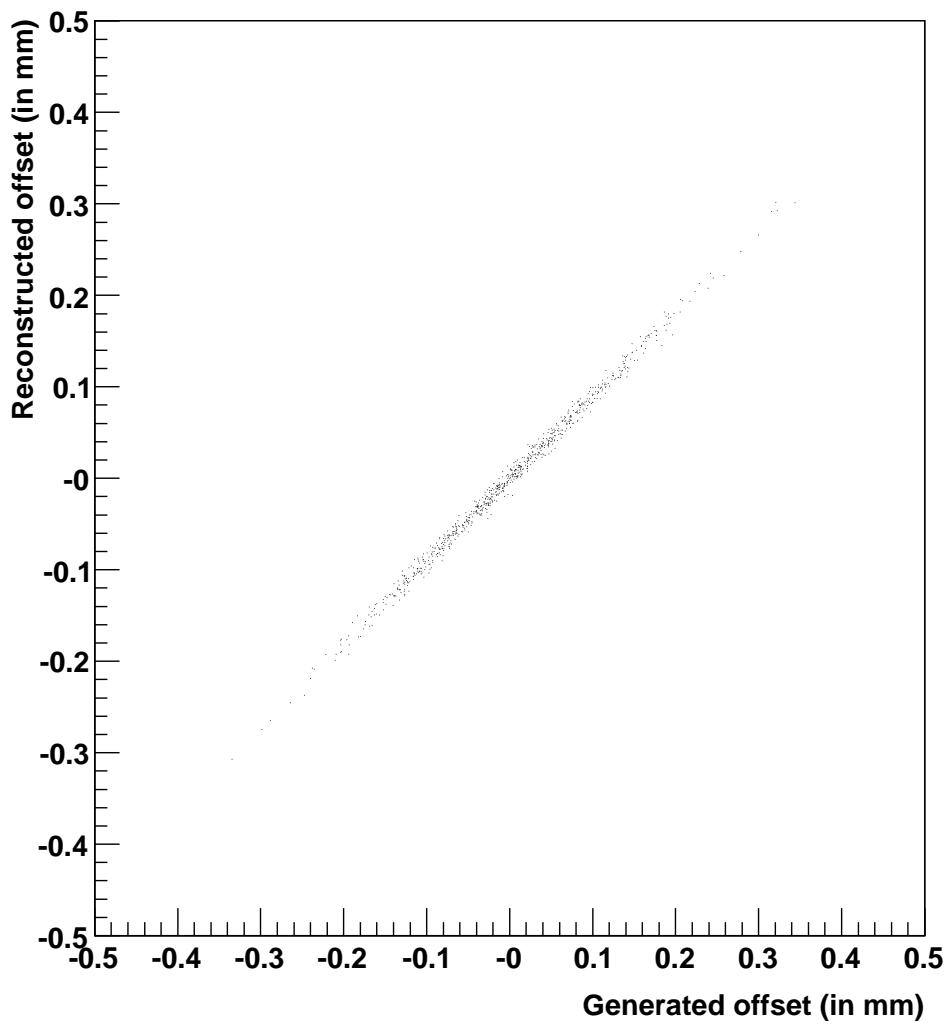
Figure 8 Box alignment robustness test: Shown are the reconstructed offset (either dx or dy) versus the corresponding generate offset (200 sets of misalignments).

LHCb Alignment Strategy
LHCb Experiment
2   VELO Alignment

Ref: *LHCb-2006-035*
Issue: *1*
Date: *June 19, 2006*
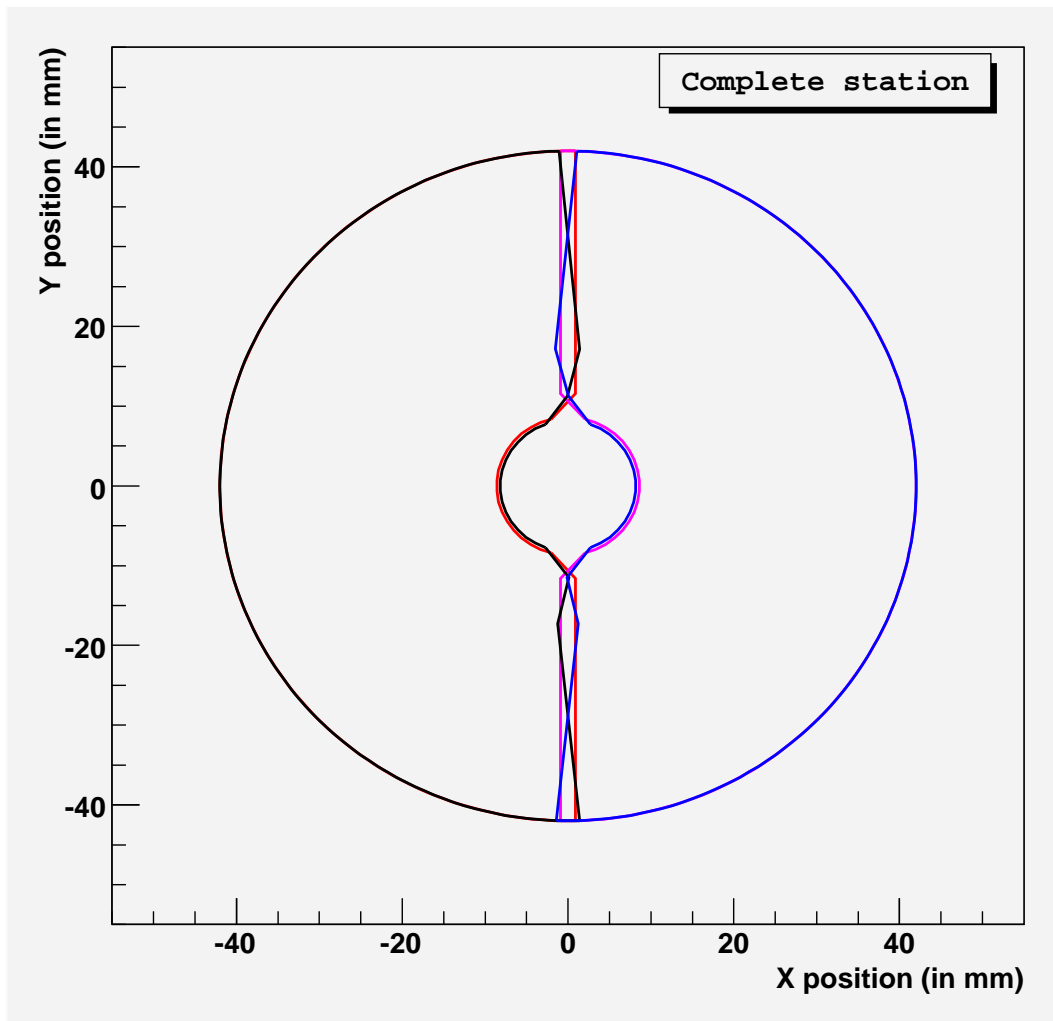
Figure 9 Overlap areas for modules within the same station: only the active silicon areas are shown. ϕ sensors are in black and blue, R sensors in pink and red

LHCb Alignment Strategy
LHCb Experiment
3   IT, OT and TT Station Alignment

Ref: *LHCb-2006-035*
Issue: *1*
Date: *June 19, 2006*
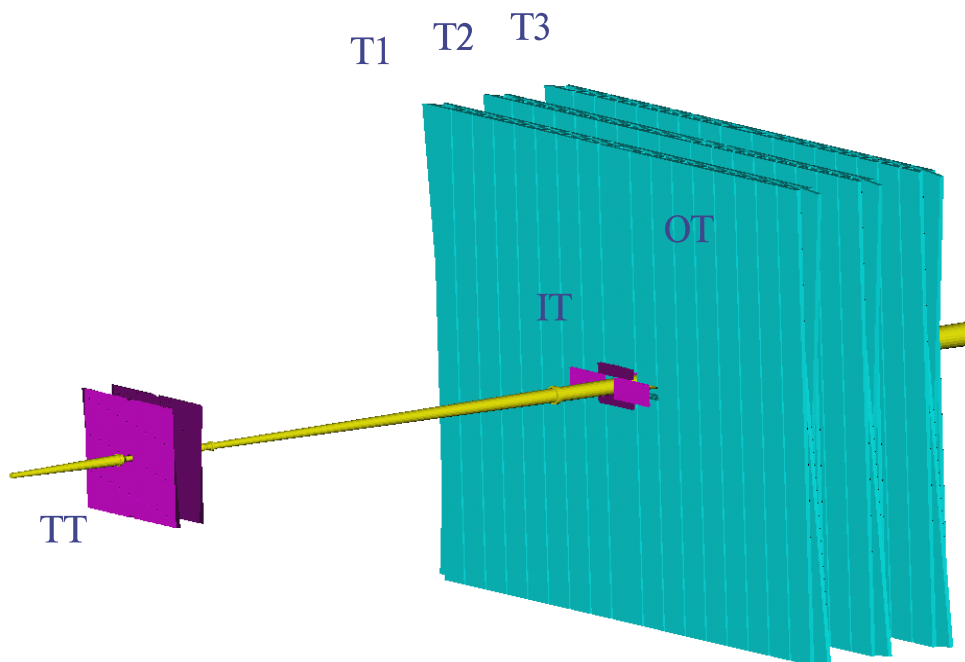
Figure 10 The main tracking system of LHCb: TT, IT and OT.

3   IT, OT and TT Station Alignment

3.1   Introduction

The charged particle tracking system downstream of the VELO consists of four stations, as shown in Fig. 10. One, the so-called Trigger Tracker (TT) station is located in front of the dipole magnet. Three other stations, referred to as the T-Stations (T1-T3), are located behind the magnet, and consist of a straw tube based Outer Tracker (OT) and a silicon strip based Inner Tracker (IT). To reach the intended momentum resolution, $\delta p/p = (0.35 - 0.55)\%$ of the tracking system, the tracking stations should be aligned so that any residual misalignments are small compared to the intrinsic resolution.

A first, coarse alignment of the spectrometer will be performed by an optical survey. The parameters derived from those measurements will be used as an initial input for the software alignment. Then, magnet-off data will be used to perform a first software alignment of the full detector. When the magnet is turned on, it is expected that small deviations from the measured positions of the tracking chambers may occur. Therefore, the spectrometer will be re-aligned with magnet-on data. In this case, the track sample for alignment purposes can be obtained by taking low-multiplicity events, and selecting from those events tracks with high momentum.

With the 1.4 m lever arm between the first and the last IT/OT stations, and the total number of detection layers of 12, internal tracking in the IT and OT is possible. This allows us to independently perform an internal alignment of these stations. Therefore, in order to align the T-stations, we will first align the OT and IT modules in each station by using internally reconstructed tracks. Then, the VELO and T-stations will be aligned with respect to each other, either simultaneously with the TT station, or without the TT. In the latter case, the TT station can be aligned in a third step, either

The internal alignment procedures of the IT and OT are expected to proceed along similar lines as discussed below. The overlap regions between the OT and the IT will allow the alignment of the OT relative to the IT (or *vice versa*).

3.2   Existing Alignment Software

As in the case of the VELO, it is foreseen to employ Millepede [15] to determine the internal alignment parameters. The underlying concept of Millepede is briefly described in Section 2.2 and we do not

LHCb Alignment Strategy
LHCb Experiment
3 IT, OT and TT Station Alignment

Ref: *LHCb-2006-035*
Issue: *1*
Date: *June 19, 2006*

repeat it here. The alignment studies discussed in this document have been performed using the Millepede code, interfaced to a simple toy MC simulation. In this version of Millepede, a χ^2 calculation is used to define the optimal solution. In the toy MC, the geometrical description of the detector is simplified to square-shaped planes of zero thickness. The only parameters are the geometrical size and the hit resolution. A hit efficiency of 100% is assumed. In addition, only translations along x and y have been considered, since translation along z and rotations introduce non-linear terms in the χ^2 calculation. Hence, matrix inversion can be used, and so the optimal solution is found by Millepede. Since this is only a toy MC simulation, the precision to which the alignment parameters are determined are not indicative of what will eventually be achieved in data. They only serve as a proof-of-principle to demonstrate the viability of the method.

In case of non-linear alignment problems, such as determining rotation angles, it is expected that an iterative approach in Millepede is feasible, provided that the non-linear parts of the equations are small enough.

3.3 Mechanical Constraints OT/IT

The Outer and Inner trackers will be supported by an aluminum platform, called the *table*, upon which are mounted three sets of rails. Each set in turn consists of three rails, where the first is used for the support structure of the IT and the remaining two rails support the C-frames upon which the OT straw tube modules are mounted.

The IT support structure and the OT C-frames are hanging from similar rails, which are mounted on a steel *bridge*. The maximally allowed deviations from the nominal position depend on the rigidity and positioning of the bridge and the table. The geometry of the bridge and the tables have been determined at Van Halteren Metaal B.V., in Bunschoten, The Netherlands by an optical survey [17]. The tolerances on the *bridge* and table construction are specified in EDMS documents [18, 19], respectively.

In these documents, tolerances on the rails are stated as follows:

    a) flatness: $3\,\mathrm{mm}$

    b) straightness: $2\,\mathrm{mm}$

Taking the rail lengths of approximately $6.55\,\mathrm{m}$, the maximal possible roll about the z-axis is $0.46\,\mathrm{mrad}$. The tilt about the y-axis is no larger than $0.3\,\mathrm{mrad}$. The tilt about the x-axis depends on the positioning of the bridge relative to the center table. Assuming that relative position of bridge and table does not induce a tilt, then the maximal possible tilt about the x-axis is given by the tolerance on the level measurement of the bridge. With a measurement accuracy of $0.5\,\mathrm{mm}$, the maximal possible tilt is about $4\mu\mathrm{rad}$. We expect that uncertainties in the positioning of the OT modules and IT boxes are much larger than those induced by the positioning of the bridge and tables.

3.4 Alignment of the Outer Tracker

The Outer Tracking is divided in three stations containing 4 measurement layers (planes) each. The stations each are $200\,\mathrm{mm}$ deep in z, and located at $z = 7838,\ 8525\ \mathrm{and}\ 9215\,\mathrm{mm}$, respectively. A more detailed description of the detector geometry can be found in [20]. The OT is constructed from straw-tubes with two layers of tubes per plane, yielding up to 24 measurements on a track. The two layers of straw-tubes are staggered by one tube radius to help resolve hit ambiguities (left or right of the anode wire). The planes are ordered in x, u, v, x', where the straw tubes in the u, v planes are tilted with respect to the y axis at an angle of $-5°$ and $5°$ degrees, respectively. Each tube contains a gold-tungsten anode wire which is $25\,\mu\mathrm{m}$ thick and consecutive wires are separated by $5.25\,\mathrm{mm}$.

A toy MC simulation has been used to study the alignment of the OT. In this toy MC, a very simple model of the OT has been implemented. Here, 12 measurement planes have been used, where a single-hit resolution of $200\,\mu\mathrm{m}$ was assumed for the straw tubes. The planes are assumed to be flat, and of zero thickness. Multiple scattering and detector inefficiencies are also ignored, in addition to the track resolution.

LHCb Alignment Strategy
LHCb Experiment
3   IT, OT and TT Station Alignment

Ref: *LHCb-2006-035*
Issue: *1*
Date: *June 19, 2006*
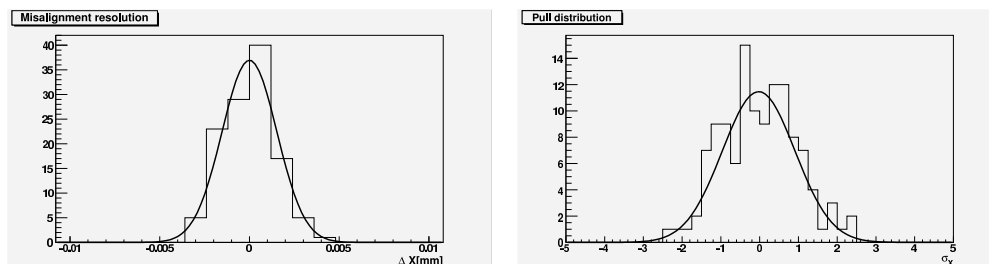
Figure 11   An example of the results of a toy MC study for the OT. Gaussian fits are overlaid as described in the text. In this particular case, a resolution on the x misalignment of 1.5 μm is found, as shown in the left panel. In the right plot, the corresponding pull distribution is shown.

As an example of such a toy MC study, the alignment procedure has been tested by applying a random shift distributed as a Gaussian with a root mean square (r.m.s) width of 3 mm to the x planes along the x direction. Here, the resolution in the misalignment parameter is calculated as the difference between the input misalignment value and the one found by Millepede. The distribution is fit to a Gaussian shape, and the mean and Gaussian width are -2.1×10^{-5} mm and 0.0015 mm, respectively. Therefore, in this toy MC simulation, the measured offset is determined with a precision of about 2 μm. As a cross-check, the pull distribution of this parameter is shown in the second panel of the figure. A Gaussian fit yields a mean of -0.027 and a Gaussian width of 1.03, indicating that the errors returned by Millepede accurately reflect the uncertainty in the extracted misalignment parameter.

Since we assumed a perfect geometry, perfect track samples were used, and multiple scattering was neglected, the alignment resolution is entirely determined by the hit resolution and the number of tracks (N_{track}) in the sample (the precision scales as $1/\sqrt{N_{\text{track}}}$). Therefore, one should not interpret the resolutions obtained with this toy MC simulation as an indication of what will be achieved with real data. Determination of alignment parameters using a full detector simulation is currently under development, and will provide a more realistic estimate of the expected resolution.

Misalignments in z and rotational misalignment introduce non-linear contributions to the χ^2 calculation. In a first approximation these terms are ignored, and as a result, the measured misalignments in z and the rotation angles are expected to depend on their input values. It is expected that this non-linear equation can be approximated by a linear equation in an iterative procedure. Such a procedure is under development, and will be implemented in Millepede. Assuming that the non-linear terms are not too large, an iterative procedure should arrive at the proper minimum in a few steps. A similar procedure was successfully used for the alignment of the HERA-B vertex detector [21].

3.5   Alignment of the Inner Tracker

The IT employs high granularity silicon strip detectors in order to deal with the large fluence of charged particles around the beam pipe (see Fig. 10). As can be seen in Fig. 12, the IT covers a cross-shaped area around the beam pipe, with dimensions of approximately 120 cm along x and 40 cm along y. In order to support the IT boxes which contain the sensors, a carbon-fiber frame is used which is hanging from from rails on the bridge and guided by rails mounted on the table.

Each IT station consists of 4 boxes, each containing 4 layers of silicon strips oriented in the same way as for the OT (x, u, v, x'). Situated in front of each OT station, the IT stations have small overlap regions with the OT straw tubes which facilitate the relative alignment of the IT with respect to the OT. In addition, there are small overlaps between the edge-sensors above and below the beam-pipe with those immediately to the left and right of the beam-pipe.

The silicon sensors are 11 cm long and 7.8 cm wide. Therefor, two sensors are glued and bonded together to cover the acceptance left and right of the beam pipe. The front of the IT stations are positioned at $z = 7628$, 8280 and 8995 mm, respectively. The boxes are 80 mm deep in z. With a pitch of 198 μm, a single-hit resolution of around 57 μm is expected.

LHCb Alignment Strategy
LHCb Experiment
3   IT, OT and TT Station Alignment

Ref: *LHCb-2006-035*
Issue: *1*
Date: *June 19, 2006*
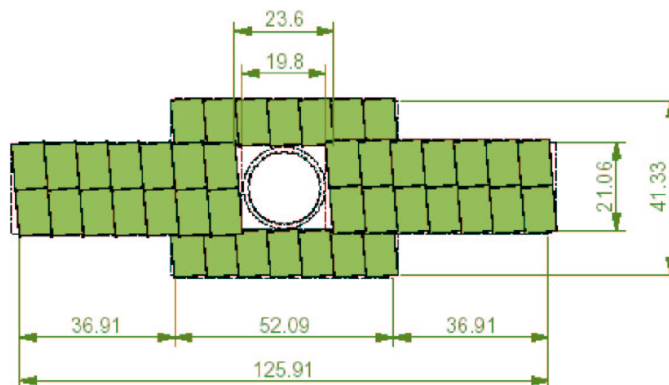
Figure 12 Dimensions of an IT layer around the beam pipe.

The boxes left and right of the beam-pipe contain the two-sensor ladders. To reduce the radiation damage induced leakage current in the sensors and provide cooling to the read-out chips, each box is employed with two cooling rods. These cooling rods also serve as support for the ladders, and therefore, each rod supports two layers of ladders (x, u) and (v, x'). The cooling rods are connected with three columns to a stiff carbon-fiber - foam sandwich. Finally, the cover plate provides the interface to the support structure.

The sensors on a ladder are positioned with respect to each other with a precision of about $10~\mu$m. The ladders are fixed to the cooling rods with a tolerance of $100~\mu$m in x and y, while the cooling rods are positioned with respect to each other no better than 0.5 mm. Therefore, it will be necessary to align individual ladders in the IT. With six degrees of freedom for each ladder, this gives a total of 2016 alignment parameters wihch will need to be determined. Finally, the precision with which the position of the cover plate will be measured is expected to be on the order of 1 mm. The accuracies on positioning and rotations are listed in Table 2.

Table 2 Maximal possible misalignments in the IT stations. Here, α, β and γ are the rotations about the x, y and z axis, respectively. Apart from the "sensors on a ladder" estimate, which is a value derived from actual measurements, all values are rough estimates. Note that only rotations about the z axis have been specified, it is expected that rotations about the x and y axes will be similar in magnitude, but as of this moment no estimates are available.

Object	tolerance	rotational constraint
sensors on ladder	$\Delta x, \Delta y = 10~\mu$m	$\gamma = 0.11$ mrad
ladders on rod	$\Delta x, \Delta y = 100~\mu$m	$\gamma = 0.6$ mrad
cooling rod to cooling rod	$\Delta x, \Delta y = 0.5$ mm	$\gamma = 1$ mrad
detector box	$\Delta x, \Delta y = 1$ mm	$\gamma = 1$ mrad

Also in the case of the IT, a simple geometric model was used in conjunction with the Millepede program. Again, sensor thickness was ignored, as well as multiple scattering and tracking resolution. Moreover, for the proof of principle, the cross-shaped geometry of the IT was simplified to rectangular-shaped planes with the dimensions of 7 double-sensor IT modules *i.e.* 530 mm in width and 220 mm in height. The planes are placed at the z position of the layers in the LHCb coordinate system and with the center of the planes at the origin of the x and y axes. In the model, a hit resolution of $57~\mu$m was assumed.

The alignment problem was kept linear, and only shifts of planes along the x and y axes were studied. We perform a large number(1000) of simulated experiments in which we shift the IT detector planes by a random amount along those axes. The shift is taken from a Gaussian distribution with a width of 3 mm. As an example, we then extract the shift in the u direction and compare it to the input value. We show in Fig. 13 the difference between the reconstructed shift in u and the input value (left panel) and the pull distribution of this variable (right panel). Gaussian shapes have been fitted to the histograms. Their means are consistent with zero and the Gaussian widths are $\sigma = 0.17~\mu$m and $\sigma = 1.01$ for the $\Delta u = u_{\mathrm{reco}} - u_{\mathrm{true}}$ and pull distributions, respectively. Therefore, in this simple toy MC

LHCb Alignment Strategy
LHCb Experiment
3 IT, OT and TT Station Alignment

Ref: *LHCb-2006-035*
Issue: *1*
Date: *June 19, 2006*
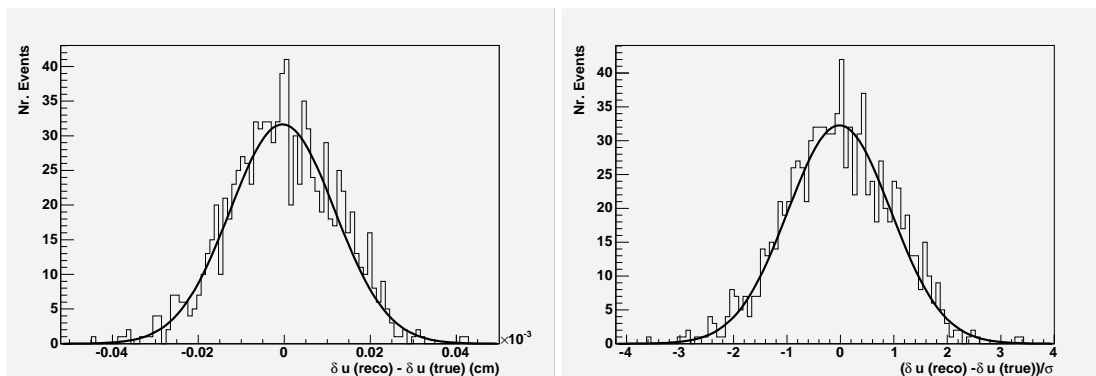
Figure 13 Alignment resolution(left) and corresponding pull distribution(right) of a stereo layer in the IT. The curves are Gaussian fits to the distributions. The Gaussian fit to the resolution distribution yields in this particular example, a mean $u = -6 \times 10^{-10}$ and a resolution of $\Delta u = \sigma = 0.17~\mu$m. The pull distribution is also fit with a Gaussian distribution, yielding a mean, $\mu = -0.03$, and width, $\sigma = 0.998$.

simulation, we extract the u offsets with a precision of about $0.17~\mu$m. This is more or less expected, given the fact that a detector resolution of $57~\mu$m and 87 k tracks were used in the calculation: $\Delta u \sim 57/\sqrt{87000} = 0.19~\mu$m. Again, we stress that these numbers should not be taken as an indication of the expected alignment precision, but rather constitute an important first step toward the implementation of alignment algorithm based on Millepede.

3.6 Alignment of the Trigger Tracker

Located in front of the dipole magnet in the fringe field of the magnet, the full acceptance is covered with silicon micro strip sensors (see Fig. 14). To cover the full acceptance, 7 sensors are glued together to form a ladder. Each ladder is split into either two or three readout sectors [22].

The TT is constructed in 2 halves, one on each side of the beam pipe. Within a detector half, each ladder will be mounted into a C-shaped frame, which is standing on a lower precision rail. Their tilt about the x-axis is determined by an upper precision rail. The mounting of TT is such that it follows the inclination of the beam axis, as opposed to IT, which is mounted vertically straight. The 2 halves can be easily retracted, or repositioned. The full support structure consisting of two pillars and two horizontal beams is fixed to the floor and to the wall of the cavern. The rails are specified to be parallel within 0.1 mm over a length of 1.9 m.

The r.m.s of the relative x offset of the sensors on a ladder has been measured to be about $10~\mu$m. From this we conclude that in the alignment we can treat each ladder as a single unit (*i.e.* we do not need to align each of the seven sensors in a ladder individually). Therefore, we need to determine 6 alignment parameters for 272 ladders. When the sensors are glued on a ladder, the sensor flatness is better than $100~\mu$m. The ladders are mounted on the cooling plate with a precision of $100~\mu$m. In Table 3, we summarize the estimates on the positioning accuracies. From this, it is concluded that each ladder will have to be aligned individually.

Table 3 Maximal possible misalignments in the TT stations. The same conventions are used as in the case of the IT. Again, only rotations about the z axis have been specified, although it is expected that rotations about the x and y axes will be similar in magnitude, but as of this moment no estimates are available.

Object	tolerance	rotational constraint
sensors on ladder	$\Delta x, \Delta y = 10~\mu$m	$\gamma = 0.11$ mrad
ladders on cooling plate	$\Delta x, \Delta y = 50~\mu$m	$\gamma = 0.35$ mrad
detector box	$\Delta x, \Delta y = 1$ mm	$\gamma = 1$ mrad

Two possible approaches to the alignment of the TT are being considered. In one approach, the ladders in the TT are aligned using full tracks, simultaneously with the alignment of the VELO relative to the

LHCb Alignment Strategy
LHCb Experiment
3   IT, OT and TT Station Alignment

Ref: *LHCb-2006-035*
Issue: *1*
Date: *June 19, 2006*
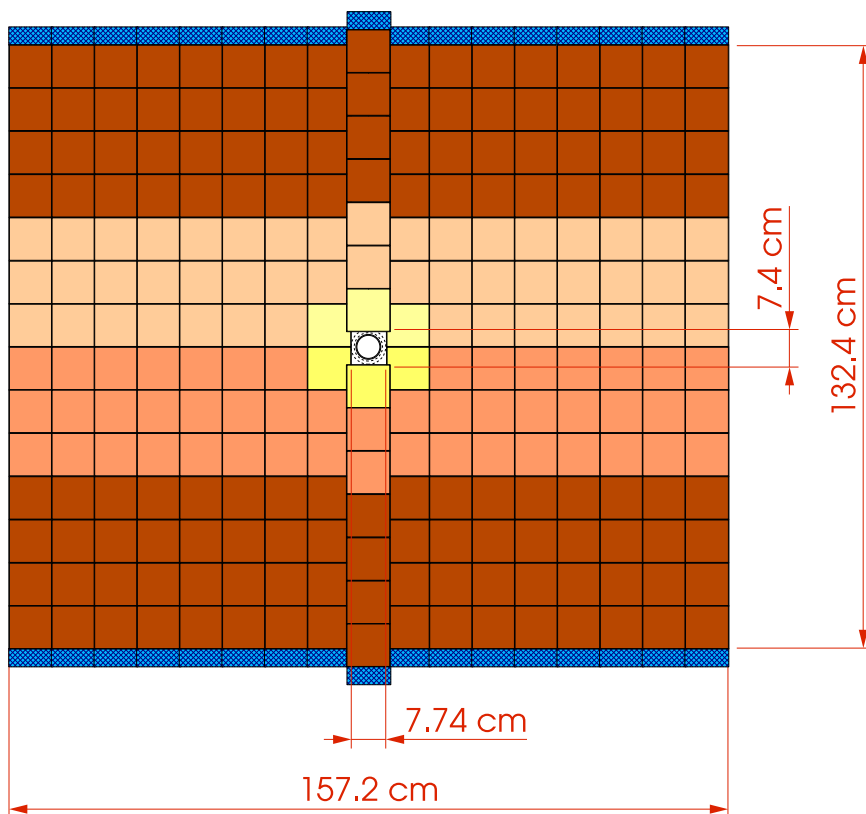
Figure 14 Schematic figure of the layout of a detection layer in the TT station.

IT and OT. In a second approach, one would align the TT ladders by computing the residuals of hits in the TT stations to tracks formed from an aligned VELO-T-Station system.

3.7   Outlook and plans

From the detector design, and when available, from measurements, some constraints on the magnitudes of the possible misalignments have been presented. Especially in the context of rotational degrees of freedom, these constraints will provide guidance for the necessary approximations needed to linearize the alignment problem.

It has been shown for an approximate IT and OT geometry that linear misalignments along x and y can be determined by using straight tracks defined by the IT and OT stations.

There remain, however several outstanding issues concerning the alignment of the T-Stations, and these will be addressed in the near future. In particular, the misalignment studies need to be extended to use the full LHCb Monte Carlo simulation, which include a proper simulation of the detector response and particle interactions. Also, the iterative procedure to extract z and rotational misalignments needs to be implemented and tested. We also need to consider that individual elements within the T-Stations will need to be aligned (*i.e.,* such as individual modules in IT and OT), thus increasing the number of alignment parameters significantly and requiring substantially more tracks to achieve a given alignment precision. Finally, alignment with the magnet switched on needs to be studied. A preliminary study has shown that curved tracks do present some non-trivial problems in the context of Millepede, and these technical details need to be addressed.

Manpower for the development of a common alignment framework has been allocated. Initially, this framework will be used to address the aforementioned open issues, moreover, it will be used to perform the alignment of the detector once it will be commissioned. Manpower for alignment studies of the TT, IT and OT has also been committed.

4　VELO to T-Station Alignment

4.1　Introduction

In this section, we describe the proposed scheme to align the detectors upstream of the dipole magnet (VELO) with the tracking detectors downstream of the magnet (T-Stations). We do not set out to use invariant mass spectra to aid in the geometrical alignment. The reasoning is that invariant masses are not only affected by misalignments, but also by inexact modeling and/or implementation of the magnetic field or small biases in the corrections to track momenta for energy loss (dE/dx) in the detector material. Both of these can produce systematic effects in invariant mass spectra, which may have dependencies on angles, momenta, etc, which could mimic misalignments. We therefore avoid the use of invariant masses for geometrical alignment, but do expect to use these spectra to calibrate the magnetic field and dE/dx corrections. This latter step is clearly done after the geometrical alignment is established.

4.2　Relative alignment between VELO and T-Stations

The relative alignment between VELO and T-Stations is first carried out with magnet off data. We then expect relatively small corrections once the magnet is turned on.

In general, there are 9 possible global transformations between the VELO and T-Stations. They are: x, y, z translations, rotations around the three principal axes (hereafter referred to as α, β and γ for x, y, z axes, respectively), and a difference in scale along the x, y, z directions. In practice the x and y scales are tightly constrained by the precisely known separation between adjacent wires or strips in a detector, and hence there are seven global alignment constants which need to be determined between these two tracking subsystems. The z-scale effect, while less often considered, represents one system being stretched or compressed with respect to the other and possible differences may arise due to the inexact knowledge of the length along the z axis of the VELO and T-Station tracking systems.

These seven global alignment parameters can all be measured using magnet off data. The technique is in principle simple and robust. One simply performs a linear projection of the x and y VELO-only tracks and the x and y T-Station-only segments to a common z location, and measure the mean deviations Δx and Δy, as well as their dependence on x and y slopes. Here, the common z is chosen to be the effective center of the magnet $z_{\mathrm{mag}} \simeq 526.9$ cm. In addition, the difference in the measured slope between VELO and T-Stations provide a direct measurement of the rotation about the x or y axes, or a z-scale effect, which should grow with increasing angle. Measurement of the global alignment parameters are therefore provided as follows:

- $\Delta\alpha$: Measure the mean difference in the y angle $\tan\theta_y^{\mathrm{VELO}} - \tan\theta_y^{T}$.

- $\Delta\beta$: Measure the mean difference in the x angle $\tan\theta_x^{\mathrm{VELO}} - \tan\theta_x^{T}$.

- y_{offset}: Measure the mean value of Δx at z_{mag}

- y_{offset}: Measure the mean value of Δy at z_{mag}

- z_{offset}: Measure the mean value of $\Delta x/\tan\theta_x$ and $\Delta y/\tan\theta_y$ at z_{mag}. Here θ_x (θ_y) are the x (y) angles of the charged particle, as measured by the VELO. For a pure z offset, one should obtain a consistent result in the two views.

- $\Delta\gamma$: Measure the mean value of the difference in azimuthal angle (ϕ) between VELO and T-Stations. Here the azimuthal angle is defined using $\phi = atan(y_{\mathrm{proj}}/x_{\mathrm{proj}})$, where x_{proj} and y_{proj} are the x and y positions of the tracks evaluated at z_{mag}, respectively.

- z-scale: Measure the mean of (a) $< \tan\theta_x^{\mathrm{VELO}} - \tan\theta_x^{T}/\tan\theta_x^{\mathrm{VELO}} >$ and (b) $< (\tan\theta_y^{\mathrm{VELO}} - \tan\theta_y^{T})/\tan\theta_y^{\mathrm{VELO}} >$. Consistent results should be obtained for a pure z scale difference.

LHCb Alignment Strategy
LHCb Experiment
4   VELO to T-Station Alignment

Ref: *LHCb-2006-035*
Issue: *1*
Date: *June 19, 2006*

In terms of order, it would make most sense to correct for slope misalignments first, since they will affect x_{offset}, y_{offset} and z_{offset}. It should be noted that the y resolution is about two times larger than the x resolution. For magnet off data, there is no bending in the $x - z$ or $y - z$ plane, and this is exploited to obtain all seven global alignment parameters. Once the field is turned on, charged particles are bent by the magnetic field. The most significant deflection is, of course, in the $x - z$ plane, but there are non-negligible fringe fields which extend into the VELO and T-Stations [1, 6, 12]. For the single-kick dipole approximation, we use the track's parameters (slopes and intercepts) obtained at the first and last measurement, which are furthest from the dipole magnet. In the $x - z$ plane, charged particles experience a momentum kick in the $x-z$ plane of about $1.23\,\text{GeV}/c$. This momentum kick doesn't only change the x slope of charged particles, but also the y slope. Defining $\vec{p}$ and $\vec{p}'$ as the momentum of a charged particle as measured in the VELO and T-stations, respectively, the $1.23\,\text{GeV}/c$ momentum kick implies $p'_x = p_x + Q \times 1.23\,\text{GeV/c}$, where $Q = \pm 1$ is the charge of the particle. To conserve momentum, p_z changes, with a value given by $p'_z = \sqrt{p_x^2 + p_z^2 - p'^2_x}$. Consequently, the y slope in the T-stations, $\tan\theta_y = p'_y/p'_z \simeq p_y/p'_z$ is also affected. For magnet on alignment, we correct for this expected change in y slope.

To test the procedure, we produce 5000 event samples of minimum bias events which are generate with one or more global alignment shifts, but reconstructed with the nominal alignments. We then demonstrate that the alignment shift that was introduced can be measured, and we can easily extrapolate the expected precision to larger event samples.

4.3   Required Precision

As discussed previously, we use the mean of a particular distribution (*ie.*, Δx) to extract the misalignment. The statistical error on this mean scales as $1/\sqrt{N_{\text{track}}}$, and hence with high enough statistics, any proposed precision (non-zero) can in principle be reached. In practice, one only needs to obtain a precision such that it has very small (negligible) impact on the physical measurables. At this time, the physics impact has not been evaluated, but one would expect that if the alignment shifts are small compared to the intrinsic resolution for the highest momentum tracks, then the impact should be negligible. To determine the intrinsic resolution, we run a simulation using perfect alignment and measure the misalignment observables for tracks with momentum larger than 40 GeV. Our criteria for an acceptable alignment is that the residual misalignment effects are no more than 5% of the intrinsic resolution, which should lead to a negligible impact on relevant physics observables. Table 4 shows the various misalignment observables, the Gaussian widths of their distributions (σ), and the widths scaled down by a factor of 20 (5%). These resolutions are achievable using a modest size event sample, as will be shown in the next sections.

Table 4 Summary of Gaussian width of the alignment observables for tracks with momentum larger than 40 GeV.

Variable	Resolution (σ)	$0.05 \times \sigma$
$\Delta\tan\theta_x$	0.2 mrad	10 μrad
$\Delta\tan\theta_y$	0.4 mrad	20 μrad
Δx	0.1 cm	50 μm
Δy	0.2 cm	100 μm
$\Delta\gamma$	11 mrad	0.55 mrad
Δz	2 cm	1 mm
z-scale (using $x - z$ view)	0.015	8×10^{-4}

4.4   Magnet OFF Simulations

We first simulate minimum bias events in the LHCb detector with the magnetic field turned off. With B=0, one does not obtain a momentum measurement from the tracking system, and low momentum tracks are not swept out of the spectrometer acceptance by the field. We therefore have many more tracks per event, as well as many more low momentum tracks which suffer from multiple Coulomb

LHCb Alignment Strategy
LHCb Experiment
4   VELO to T-Station Alignment

Ref: *LHCb-2006-035*
Issue: *1*
Date: *June 19, 2006*

scattering in the detector material. While this will degrade the matching resolution between VELO and T-Station segments, it does not produce a bias in the mean, and therefore is not critical. If necessary, we could select tracks which have a matching shower in the electromagnetic and hadronic calorimeters which exceed some threshold ($\approx$10 GeV). Here, we do not apply any requirement on matching energy in the calorimeters.

Here we define several 5000 event samples of simulated events. In each sample, we apply one or more global transformations to the VELO. We also use the same random number generator for each sample, so the generated events are identical, and only the effect of alignment offsets differ between each sample. The samples are defined as follows:

- Sample 1A: Perfect Alignment

- Sample 2A: x_{offset} = -1 mm

- Sample 3A: y_{offset} = -5 mm

- Sample 4A: z_{offset} = 10 mm

- Sample 5A: $\Delta\gamma$ = 2 mrad

- Sample 6A: Rotation: $\Delta\alpha = \Delta\beta = 0.5$ mrad, $\Delta\gamma = 2$ mrad, Δx=0.25 mm, Δy=-0.25 mm, Δz=5 mm.

As an example of the distributions for several of the alignment parameters, we show results obtained using perfect alignment in Fig. 15. The distributions are as follows: (a) the difference in x slopes as measured by the T stations and the VELO, (b) the difference in y slopes as measured by the T stations and the VELO, (c) $\Delta x \equiv x_{\text{VELO}} - x_{\text{T}}$ evaluated at z_{mag}, (d) $\Delta y \equiv y_{\text{VELO}} - y_{\text{T}}$ evaluated at z_{mag}, (e) $\Delta\gamma \equiv \Delta x/\tan\theta_y^{\text{VELO}}$, and (f) $\Delta z = \Delta x/\tan\theta_x^{\text{VELO}}$. We fit each distribution to the sum of two Gaussian's whose means are constrained to a common value to describe the signal portion and a linear term for the background. The fitted means are summarized in the row labeled "Sample 1A" in Table 5. All fit values are consistent with a mean of zero as expected. The precision to which these offsets are determined are small compared to the intrinsic resolution. In the case that higher precision is needed, the uncertainties on the mean in Table 5 will be reduced by roughly $\sqrt{N/5000}$ for N minimum bias events.

Similarly, the other rows show the fitted means for several other applied misalignments. The parameters which are misaligned have a superscripted star, where the input values are given above. With the exception of Sample 6A, all input misalignments are well determined. For Sample 6A, the rotations $< \Delta\alpha >$, $< \Delta\beta >$, $< \Delta\gamma >$, and Δz are correctly extracted, but $< \Delta x >$ and $< \Delta y >$ are biased as expected. This is simply because if one rotates the VELO by $\Delta\alpha = 0.5$ mrad about the y axis, then a shift in Δx of $\Delta x = \Delta\alpha \times (z_{\text{mag}} - z_{\text{VELO}}) \sim 2.6$ mm results. This is consistent with what is observed. This illustrates the need to first correct for rotations around the x and y axes before addressing $< \Delta x >$ and $< \Delta y >$.

Table 5   Summary of the fitted means for the seven alignment parameters under several applied misalignments using 5000 simulated minimum bias events with the magnet off. Quantities with a * indicate the parameters which were intentionally misaligned.

Trans- form.	$< \Delta x >$ (μm)	$< \Delta y >$ (μm)	$< \Delta z >$ (cm)	$< \Delta\alpha >$ (μrad)	$< \Delta\beta >$ (μrad)	$< \Delta\gamma >$ (mrad)	$< z_{\text{scale}}^x >$ (10^{-3})
1A	16 ± 22	-57 ± 50	0.04 ± 0.08	7 ± 7	-7 ± 10	0.15 ± 0.15	0.01 ± 0.28
2A	$-956 \pm 25^*$	-51 ± 40	0.06 ± 0.09	12 ± 7	-4 ± 12	0.06 ± 0.15	0.07 ± 0.27
3A	48 ± 29	$-4959 \pm 50^*$	0.50 ± 0.10	18 ± 7	4 ± 17	0.24 ± 0.22	0.58 ± 0.30
4A	11 ± 26	32 ± 52	$1.25 \pm 0.10^*$	-5 ± 8	-13 ± 11	-0.01 ± 0.16	0.39 ± 0.28
5A	-31 ± 24	11 ± 45	0.09 ± 0.09	-4 ± 7	12 ± 10	$2.03 \pm 0.23^*$	0.32 ± 0.27
6A	$2385 \pm 27^*$	$2878 \pm 37^*$	$0.58 \pm 0.16^*$	$502 \pm 7^*$	$494 \pm 14^*$	$1.90 \pm 0.18^*$	-0.32 ± 0.40

LHCb Alignment Strategy
LHCb Experiment
4   VELO to T-Station Alignment

Ref: *LHCb-2006-035*
Issue: *1*
Date: *June 19, 2006*
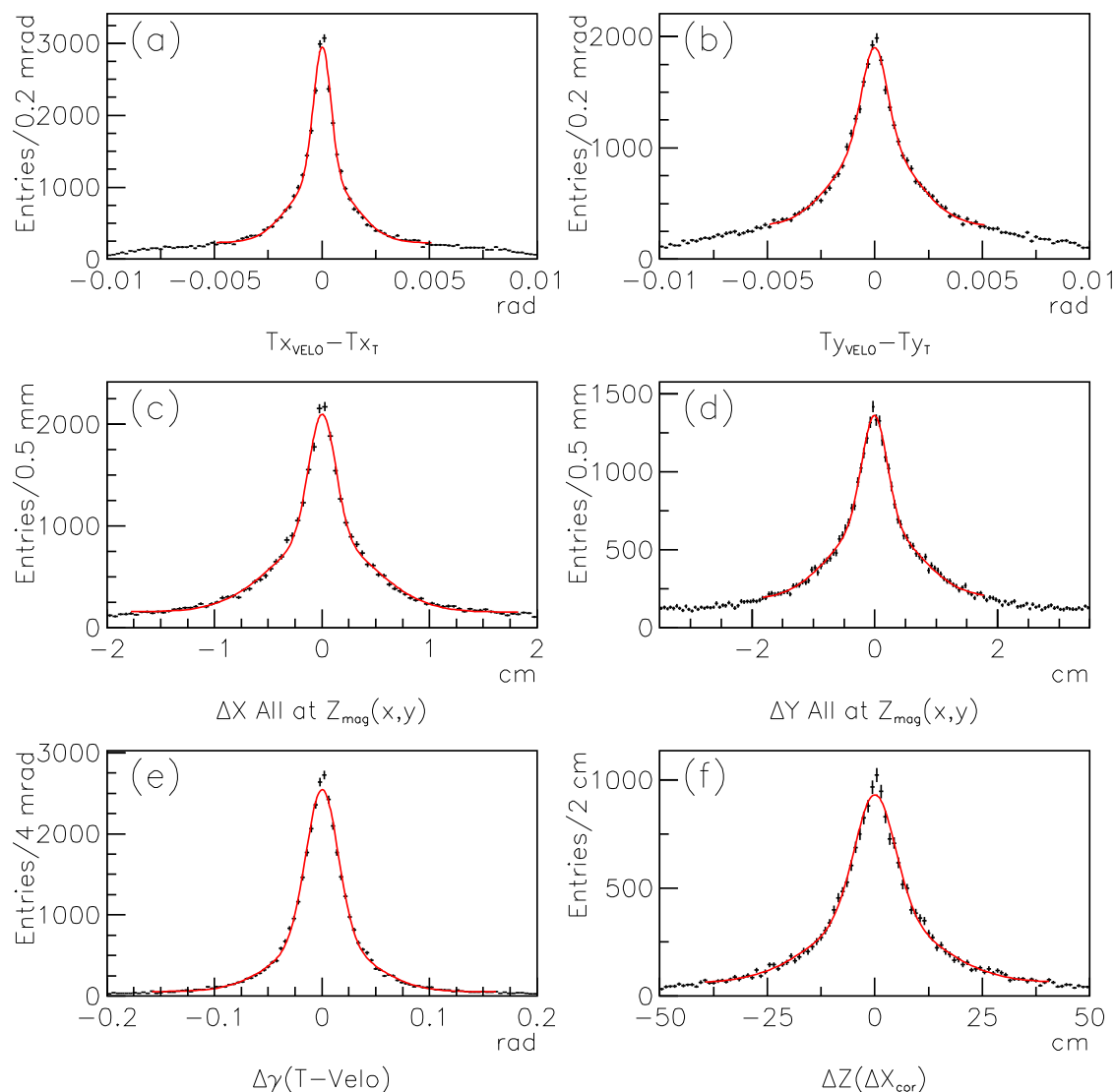
Figure 15 Several distributions related to the relative alignment between the T-Stations and VELO for perfect alignment. The distributions show: (a) the difference in x slopes as measured by the T stations and the VELO, (b) the difference in y slopes as measured by the T stations and the VELO, (c)$\Delta x \equiv y_{\mathrm{VELO}} - y_{\mathrm{T}}$ evaluated at z_{mag}, (d) $\Delta y \equiv y_{\mathrm{VELO}} - y_{\mathrm{T}}$ evaluated at z_{mag}, (e) $\Delta\gamma \equiv dx/\tan\theta_y^{\mathrm{VELO}}$, and (f) $\Delta z = \Delta x/\tan\theta_x^{\mathrm{VELO}}$. The histograms are simulated data and the smooth curves are fits as described in the text.

LHCb Alignment Strategy
LHCb Experiment
4   VELO to T-Station Alignment

Ref: *LHCb-2006-035*
Issue: *1*
Date: *June 19, 2006*

4.5   Magnet ON Simulations

In general, the simple *single kick* approximation to the dipole field is not exact, and significant dependencies on entrance and exit angles as well as momentum are expected. Since we are only seeking 7 global alignment parameters, we can be selective of tracks in order to minimize this dependence. In particular, we require charge particles to have momenta larger than 20 GeV/c, have x and y angles in the VELO less than 100 mrad, and an x slope in the T-Stations of less than 200 mrad (the y slope in the T-Stations is nearly equal to the y slope in the VELO, so no additional requirement is made.) After these charged particle selection, we apply two corrections: the first is a correction for the expected change in the y slope (discussed in Section 4.1), and the second is a correction for the x angle in VELO. The y slope correction is given by $\delta \tan \theta_y = -0.0029 \times \tan \theta_y^{\mathrm{VELO}}$. The change in y slope is coupled with a corresponding change in y intercept, which is obtained by pivoting the track about the center of the T-Stations ($z \approx 850$ cm), *ie.*, $\delta\, y_{\mathrm{int}} = 850$ cm $\times\, \delta \tan \theta_y$. The x angle correction is one which accounts for the entrance angle of the track in the $x - z$ plane. As the x angle increases, it tends to move the effective z_{mag} to smaller z values. This latter correction is derived from a simulation of the LHCb dipole magnet using perfect geometry and the measured field map. The correction to z_{mag} is parameterized as $\delta z_{\mathrm{mag}} = 1.6 \tan \theta_x^{\mathrm{VELO}} - 200.0 \tan \theta_x^{\mathrm{VELO}\, 2}$. Since most of the tracks populate the low angle regions, the latter correction, which does depend on the field map can be removed with only a small bias in the reconstructed alignment parameters. Also, it should be measurable using data.

Here again we use several 5000 event samples of simulated events. In each sample, we apply one or more global shifts to the VELO. We also use the same random number generator for each sample, so the generated events are identical, and only the effect of alignment offsets differ between each sample. The samples are defined as follows:

- Sample 1B: Perfect Alignment

- Sample 2B: x_{offset} = -1 mm

- Sample 3B: y_{offset} = -5 mm

- Sample 4B: z_{offset} = 10 mm

- Sample 5B: $\Delta\gamma$ = 2 mrad

- Sample 6B: $\Delta\alpha$ = 0.5 mrad

- Sample 7B: Δx=-0.25 mm, Δy=0.25 mm, Δz=4.0 mm, $\Delta\gamma$=2 mrad

The same analysis as for magnet off simulation is carried out with magnet on simulation, except in this case extraction of $\Delta\beta$ (rotation around the y axis) is difficult, if not impossible, to extract from geometry alone because it is equivalent to introducing a small additional bend angle in the bend plane of the magnet. This simply changes the measured momentum of the particle. On the other hand, it is unlikely that an overall rotation of the VELO or T-Station system would occur when turning on the magnet. In its place, we show the mean z intersection point of all pairs of charged particles under the various misalignment scenarios. Secondly, the measurement of differences in z_{scale} with magnet off data took advantage of the non-bending in the $x - z$ plane, which is not applicable to magnet on simulation, and therefore we use the $y - z$ projection. While the resolution is the $y - z$ projection is worse by a factor of two than the $x - z$ view, it is unlikely that turning on the magnet will introduce a significant change of z-scale. The results of the various misalignment scenarios are tabulate in Table 6.

As with the magnet off data, we find that the measured misalignments are generally consistent with their input values. (Again we highlight in bold the parameters which were intentionally misaligned.) As with the magnet off simulation, one finds that when we introduce a rotation around the x axis, this introduces a systematic shift in $< \Delta y >$. Again, one would need to correct for this large relative tilt before addressing the translation.

We also note that the center of magnet, does not change significantly with the applied misalignments. This is encouraging, since computation of Δx requires us to know the center of the magnet. Therefore, even with a moderate relative misalignment between VELO and T-Stations, the center of the magnet can be reliably determined directly from the data and cross-checked with the simulation.

LHCb Alignment Strategy
LHCb Experiment
4   VELO to T-Station Alignment

Ref: *LHCb-2006-035*
Issue: *1*
Date: *June 19, 2006*

Table 6 Summary of the fitted means for the six of the alignment parameters under several applied misalignments using 5000 simulated minimum bias events with the magnet on. The mean intersection point of all pairs of VELO and T-Station tracks is also indicated. Quantities with a * indicate the parameters which were intentionally misaligned.

Trans-form.	$< \Delta x >$ (μm)	$< \Delta y >$ (μm)	$< \Delta z >$ (cm)	z_{mag} (cm)	$< \Delta \alpha >$ (μrad)	$< \Delta \gamma >$ (mrad)	$< z_{scale}^{y} >$ (10^{-3})
1B	-30 ± 22	75 ± 47	0.11 ± 0.10	526.6 ± 0.1	-10 ± 14	0.47 ± 0.30	-1.0 ± 1.4
2B	$-1036 \pm 23^*$	52 ± 49	-0.09 ± 0.15	526.7 ± 0.1	-11 ± 15	0.40 ± 0.31	-1.0 ± 1.2
3B	101 ± 31	$-5049 \pm 71^*$	0.42 ± 0.13	526.7 ± 0.1	-11 ± 22	1.15 ± 0.73	-0.3 ± 1.7
4B	-29 ± 22	-73 ± 51	$1.07 \pm 0.11^*$	526.9 ± 0.1	29 ± 15	0.57 ± 0.28	-0.8 ± 1.2
5B	-11 ± 23	-30 ± 50	0.08 ± 0.11	526.8 ± 0.1	-2 ± 15	$2.56 \pm 0.28^*$	0.5 ± 1.2
6B	6 ± 22	2613 ± 51	0.15 ± 0.11	526.8 ± 0.1	$487 \pm 14^*$	-0.60 ± 0.38	1.5 ± 1.4
7B	$-254 \pm 23^*$	$200 \pm 54^*$	$0.32 \pm 0.13^*$	526.7 ± 0.2	37 ± 15	$2.38 \pm 0.33^*$	-2.4 ± 1.2

4.6   Relative VELO T-Station Alignment Summary

These simulations indicate that relative misalignments between the VELO and T-Stations can be extracted with no observable bias. A sample of roughly 5000 events should be sufficient to obtain a reasonable precision on the misalignment parameters. A reduction in the uncertainty can be obtained using larger sample sizes, and one can scale the quoted errors by $1/\sqrt{N_{ev}}$. As the statistical errors are reduced, systematic effects, such as detector asymmetries, mis-modeling of the field, tracking biases, etc, may produce a non-zero mean of the relevant distribution. During the initial commissioning of LHCb we should expect to have a very large sample of magnet off data, and this sample may help illuminate some of these biases (which can then be understood and corrected). It is clear that small biases may remain, and as long as they are well below the $O(1\%)$ level of the intrinsic resolution, it is inconceivable that they would significantly bias any physical measurements. Therefore, during regular LHCb running, we expect the misalignment parameters to be determined to a precision at the level of (1-2)% of the intrinsic resolution using the techniques described in the preceding sections. Once the full tracking system is aligned, these tracks can be used to align the RICH, ECAL, HCAL and MUON by selecting a suitable subsample of tracks. For example, in the RICH, one can select charged particles which have $\beta = v/v \simeq 1$. For the ECAL alignment, one can use electrons from photon conversions, or at the higher momentum, one can use electrons from $J/\psi \rightarrow e^+ e^-$, although this will require a longer running time. The muon system can choose tracks that pass through all 5 Muon Stations, or if there is sufficient statistics, muons from J/ψ decay can be used. The hadron calorimeter can use high energy hadrons. Once these subsystems are brought into alignment with the tracking system, the detector is aligned. The translation to the absolute LHCb global frame will use the readback of the VELO motion controller. Thus, once all these steps are performed, all active detector elements will be located in the LHCb global frame.

LHCb Alignment Strategy
LHCb Experiment
5 RICH Alignment

Ref: *LHCb-2006-035*
Issue: *1*
Date: *June 19, 2006*

5 RICH Alignment

5.1 Introduction

The accurate reconstruction of the Cherenkov angle for each photon from a given track in the Ring Imaging Cherenkov Detector (RICH) systems assumes accurate knowledge of the geometry and orientation of the mirror panels, the individual mirrors, the HPD boxes and the individual HPDs in RICH1 and RICH2. There are 4 spherical and 16 secondary mirrors in RICH1, and 56 and 40, respectively, in RICH2. The total number of HPDs in both detectors is 484. RICH2 has already been installed in the LHCb experimental area and the alignment of the mirrors has been measured. Although the exact orientation of the mirror panels has not been measured, the misalignment of the individual mirror segments from forming a single mirror is below 0.2 mrad. The aim of the RICH group is to keep the alignment contribution to the Cherenkov angle resolution after software corrections below 0.1 mrad. This is to be compared to 1.27 mrad per photoelectron (for RICH1) from other sources, of which ∼0.5 mrad is from tracking resolution.

5.2 Basic principles

Cherenkov photons emitted in the radiator from each particle track are distributed on a ring on the photo-detector surface, with the radius representing the Cherenkov angle and the centre given by the track. Any misalignment, either internal, or between the RICH and the tracking system, has the result of moving the circle with respect to the assumed centre, as in Figure 16 where *all distances represent angles*. The real centre of the circle is C, but the point given by the projection of the track is C′. So the measured Cherenkov angle is ϑ_{ch}, while the real Cherenkov angle is ϑ_0 [23].

$$\vartheta_{ch} - \vartheta_0 = dcos(\phi_{ch} + \phi_0) \quad \text{or}$$

$$\vartheta_{ch} - \vartheta_0 = acos(\phi_{ch}) + bsin(\phi_{ch}) \tag{3}$$

Distance d represents the angle of the mirror segment tilt, and a and b the tilt projections onto the x and y axes, respectively. Plotting $\vartheta_{ch} - \vartheta_0$ against ϕ_{ch} can reveal this misalignment and by fitting the curve a and b can be extracted. Selecting only high momentum (saturated) tracks can ensure that the real angle is known. It has to be stressed that the analysis is done on a photon by photon basis. There is no requirement for an actual ring.

In practice, it is not possible to associate with certainty a Cherenkov photon to a particular track. A probability for a photon to come from a particular track can be calculated and the most unlikely
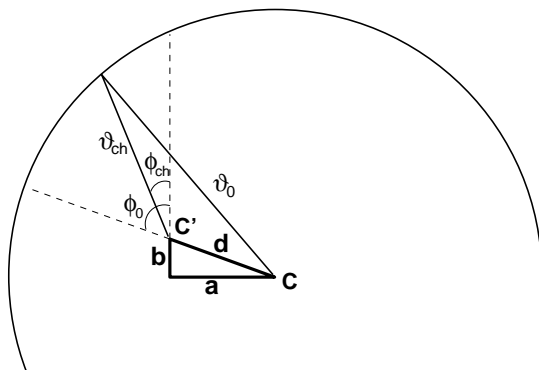

Figure 16 A Cherenkov ring on the detection plane resulting from mirror misalignment. Photons are distributed on the circle. Point C is the real centre of the circle, however point C', derived from the track, is used to calculate the Cherenkov angle ϑ_{ch}. The distances ϑ_0, ϑ_{ch}, a, b and d represent Cherenkov angles and the mirror tilts.

LHCb Alignment Strategy
LHCb Experiment
5   RICH Alignment

Ref: *LHCb-2006-035*
Issue: *1*
Date: *June 19, 2006*

photons can be rejected, but not all. So, any effort to plot $\Delta\vartheta_{ch}$ with respect to ϕ_{ch} will contain a significant number of *background* photons, namely, photons that originated from a different track. However, the Cherenkov angle for these photons has a flat distribution and they can be subtracted. Figure 17 shows a plot of $\Delta\vartheta_{ch}$ versus ϕ_{ch}, where the mirrors of RICH2 have been misaligned. After background subtraction and fit, the mirror alignment parameters can be extracted. A proof of principle study for the alignment of the RICH mirrors has been performed successfully, and has set a maximum deviation for the various mirror segments from forming an ideal mirror to 0.5 mrad [24].

5.3   RICH alignment strategy

As mentioned in the introduction a number of different components of each of the RICH detectors will have to be aligned. These include, individual HPDs, each HPD box, individual mirror segments, the panels holding the mirrors and finally the RICH detectors themselves with respect to the rest of the LHCb experiment. The mechanical tolerance of the various components is of the order of 1 mm, which will permit the operation of the detector to a reasonable standard at the start of the experiment. The final alignment is expected to be performed using charged tracks in data, after the alignment of the tracking system. For the studies done so far, we have assumed that residual misalignments in the tracking system (after the tracking system has been aligned) are much smaller than the intrinsic tracking resolution, and thus we assume a perfectly aligned tracking system. More detailed studies of the impact of aligning the RICH with an imperfectly aligned tracking system will be investigated. We have assumed that the orientation of the silicon sensors with respect to the HPD axis is determined from bench tests by illuminating the HPD with a fixed input pattern. We also assume that the relative position of the tubes within the HPD array are determined in-situ from an external calibration system, which is currently being designed. This system is necessary to unfold the magnetic field distortions (see Section 5.5), and should also be able to provide a position map of the HPD tubes.

A laser and camera system will monitor a subset of the mirror segments for possible movement, especially if there is any temperature change and during the powering of the magnet.

The alignment of the various components with data will be performed with the technique described in section 5.2. The drawback of the technique is that only one misalignment component can be identified at a time, so the data must be selected in such a way as to include only one misalignment element. For example in the mirror misalignment study [24] photons reflected from a particular mirror segment combination (spherical, secondary) were selected.

It is expected that selecting the data in this way can reveal the various levels of misalignment, from a whole RICH detector to individual HPDs. For example, the relative positions of the HPDs can be calculated by fitting the Cherenkov circles (rings) after enough data has been collected to illuminate the entire HPD. This will happen very quickly for the HPDs in the central region, but may require collecting data for hours or days for the HPDs at the edges.

The alignment can also be verified by selecting isolated rings where the probability for all the photons to have originated from the same track is very high. These rings can the be tested for continuity.

5.4   RICH mirror segments

The alignment of the RICH mirrors is a special case. Both RICH detectors use a two mirror system, so a two stage process is necessary to extract the mirror tilts. First, a different histogram must be filled for every spherical/secondary mirror combination (i, j) to extract the parameters a and b. These parameters give the added tilt of the two mirrors in each combination. The second stage is to extract the parameters for the individual segments by minimizing a function of the form:

$$\sum_{i,j} \left[(a_{ij} - x_i - x_j)^2 + (b_{ij} - y_i - y_j)^2 \right] \tag{4}$$

where i counts the spherical segments, j the secondary mirror segments, a and b are the measured total tilts and x and y are the tilts of individual mirror segments along the x and y axes. With this procedure it is possible to align the mirrors relative to one mirror segment, but not absolutely as any tilt of the

LHCb Alignment Strategy
LHCb Experiment
5   RICH Alignment

Ref: *LHCb-2006-035*
Issue: *1*
Date: *June 19, 2006*
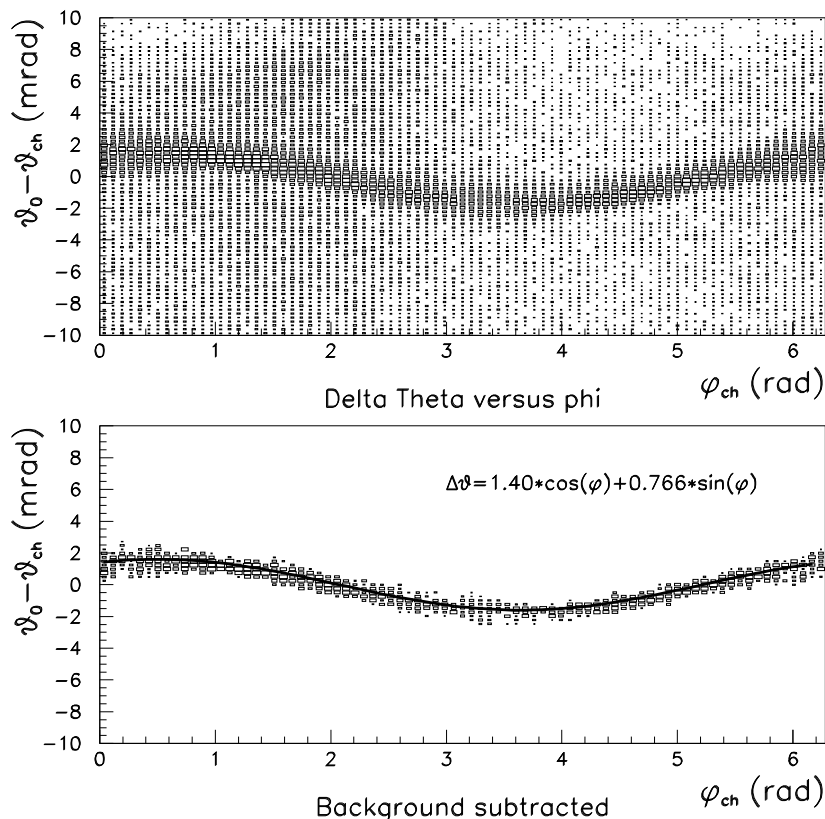
Figure 17 A 2D histogram of $\Delta\vartheta$ against ϕ_{ch}. The background was subtracted by applying a cut at 30% of the maximum on each column separately and the result of the fit is shown.

spherical mirrors can be compensated by assuming an equivalent tilt in the opposite direction of the secondary mirrors.

In practice, the bias on the measured Cherenkov angle depends on the geometry and the path followed by the photon. The longer the photon path to the detection plane after it has hit a particular mirror segment, the bigger the bias if this particular mirror is misaligned. Since every mirror combination has a limited acceptance of photon angles, it is possible to measure a magnification coefficient for each mirror, using the LHCb Monte-Carlo simulation. This magnification coefficient is important because the photon path after the spherical mirrors is longer compared to the path after the secondary mirrors, so the spherical mirrors cause a bigger bias to the Cherenkov angle for the same misalignment angle. Equation 4 can be changed to:

$$\sum_{i,j} \left[\frac{(a_{ij} - p_{ij}^x x_i - q_{ij}^x x_j)^2}{\sigma_{a_{ij}}^2} + \frac{(b_{ij} - p_{ij}^y y_i - q_{ij}^y y_j)^2}{\sigma_{b_{ij}}^2} \right] \tag{5}$$

to include the magnification coefficients p and q and the errors in the measurement of a and b. The magnification coefficients have both indices i and j because they depend on the mirror segment combination and not on the individual spherical or secondary mirror segment, as the total magnification depends on the geometrical path that was followed. This expression can then be minimized using MINUIT [25], or a similar program, to fit x_i, x_j, y_i and y_j and extract all the mirror tilts relative to a chosen mirror segment.

LHCb Alignment Strategy
LHCb Experiment
5 RICH Alignment

Ref: *LHCb-2006-035*
Issue: *1*
Date: *June 19, 2006*

5.5 Magnetic field distortions

The operation of the HPDs in a magnetic field (the fringe field of the main LHCb magnet) is expected to cause distortions due to the Lorentz forces on the photoelectrons (Figure 18). These distortions have been studied, are well understood [26] and will be corrected. Systems are currently being developed that will project a geometric pattern on the HPD plane so that a map of pixel positions to photo-cathode positions can be created. It is expected that these systems will operate initially with the magnet off in a distortion free environment, and that they will be operational while the magnet is being powered. This enables the extraction of a magnetic distortion map in an unambiguous way.

The distortions due to the magnetic field are closely related to alignment, as they can move the effective centre of an HPD. For this reason the corrections will be part of the alignment strategy of the RICH. Taking data without a magnetic field is part of this strategy. Procedures for identifying saturated rings without momentum information from the tracking are being investigated. These include high energy pions identified by the calorimeter and muons found by the muon system.

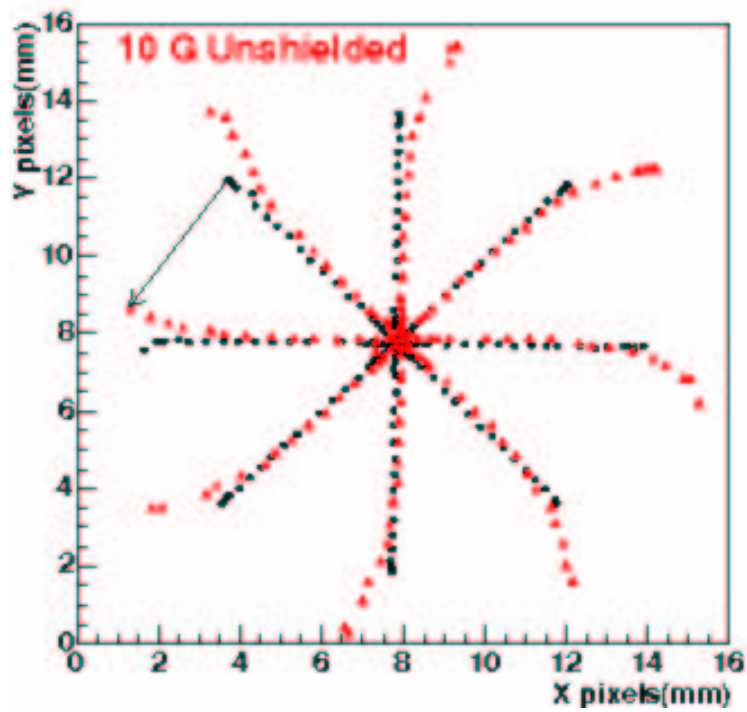**LHCb Alignment Strategy**
LHCb Experiment
5   RICH Alignment

Ref: *LHCb-2006-035*
Issue: *1*
Date: *June 19, 2006*

Figure 18 Distortion of an image on the HPD anode due to a 10 Gauss magnetic field parallel to the HPD axis.

LHCb Alignment Strategy
LHCb Experiment
6   Calorimeter Alignment

Ref: *LHCb-2006-035*
Issue: *1*
Date: *June 19, 2006*

6   Calorimeter Alignment

6.1   Calorimeter architecture

The calorimeter subsystem for LHCb consists of four consecutive semi-projective detectors. Upstream, the Scintillator Pad (SPD) and the Preshower (PS) detectors are intended to aid in distinguishing electromagnetic from hadronic showers, as well as provide discrimination between electron and photon-induced showers. Downstream, the electromagnetic (ECAL) and hadronic (HCAL) calorimeters measure the energy and position of showering particles.

The hadronic calorimeter is comprised of about 1500 pads with two regimes of transverse segmentation, increasing from the inner ($\sim 13 \times 13\ cm^2$) to the outer region ($\sim 26 \times 26\ cm^2$). The HCAL pads are assembled in horizontal modules. The overall HCAL structure consists of two lateral halves, one on each side of the beam-pipe, each formed from a wall of those horizontal modules placed on a mobile support chariot.

The electromagnetic calorimeter is made of about 6000 scintillator pads with three regimes of transverse segmentation increasing from $\sim 4 \times 4\ cm^2$ at the innermost section to $\sim 12 \times 12\ cm^2$ at the outermost region. The ECAL pads are assembled in square modules with dimension 121.7×121.7 mm^2. Like the HCAL, the overall ECAL structure is composed of two lateral halves, each forming a wall of those square modules placed on a mobile support chariot.

The preshower and SPD segmentation have been designed to have a one-to-one correspondence with the ECAL pads. Those pads are assembled in 8 vertical super-modules and are mounted on the support beam for the first muon station (M1).

6.2   Hardware measurement and positioning

Accurate measurements of the ECAL and HCAL positioning have been achieved during their installation in 2005. Fiducials and geometrical measurements are documented in several EDMS notes [28]. The main points are list here :

- Horizontality : the horizontality of both the ECAL and HCAL support chariots have been measured to be within the measurement precision (± 0.2 mm).

- Verticality : the z-position of the ECAL modules have been measured at 390 points on the ECAL front side to be within ± 2 mm. The HCAL front side vertical is within 0.5 mm.

- Transversal size : the transverse ECAL wall size is within measurement error to the design value . The (x, y) transverse positions of the modules are known to 0.5 mm.
  The tolerance of the HCAL horizontal modules are within ± 1.5 mm as illustrated in Fig. 19.

- Height (Y) positioning : the Y-position of the ECAL halves had been measured to be 1.29 mm and 1.99 mm lower than their nominal position for the $+x$ and $-x$ side, respectively.

- Lateral (x) positioning : Both halves of the ECAL and HCAL are mobile in the x-direction. The motorized closing of the two halves will be monitored via the Experiment Control System with a precision at the millimeter level .

To summarize, both the ECAL and HCAL halves can be considered as monolithic walls of which the position and the size are accurately known. Once the two halves are closed, the structure is not expected to suffer from any deformation.

The vertical super-modules for the SPD and for the PS have been assembled and will be installed in the coming weeks in the LHCb cavern. Each super-module will be independent of its neighbors in order

LHCb Alignment Strategy
LHCb Experiment
6 Calorimeter Alignment

Ref: *LHCb-2006-035*
Issue: *1*
Date: *June 19, 2006*
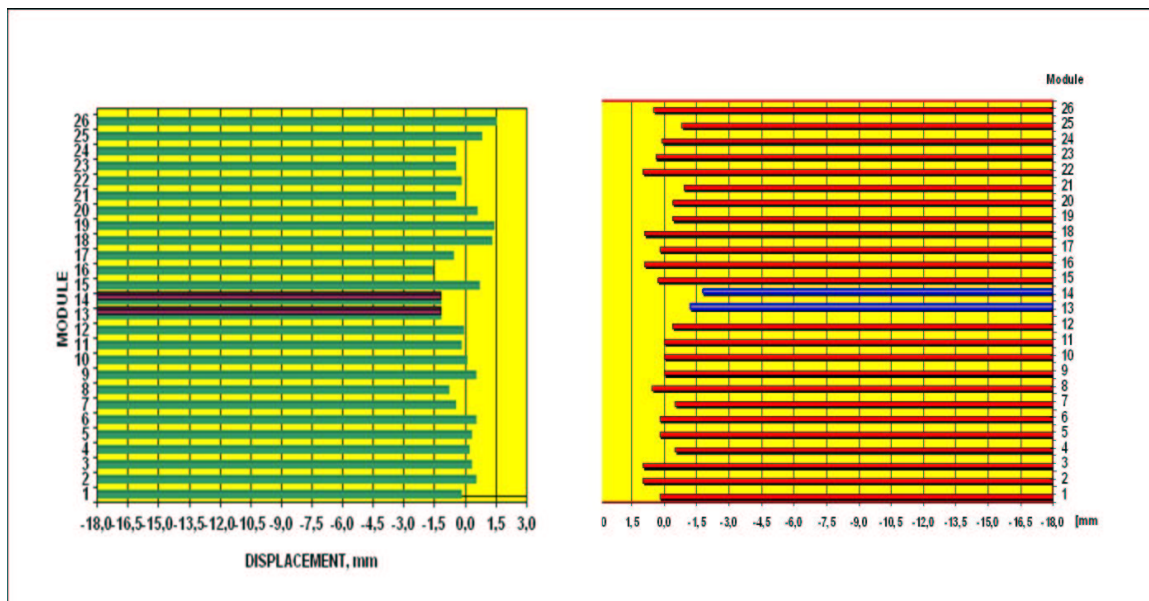
Figure 19 HCAL modules alignment. The abscissa indicates the minimum-average displacement (mm) for the $+x$ calorimeter half (left) and the $-x$ calorimeter half (right).

to ensure that the structure can support the possible individual vertical displacements due to possible deformation of the support beam that could occur when opening the system (including M1). The opening/closing of the two halves of the SPD and the PS devices will be based on the same precision motorization as used for the ECAL and the HCAL.

6.3 Resolutions

The purpose of the calorimeter system is two-fold. First, it provides high transverse energy electron, photon, π° and hadron candidates to the Level-0 trigger system. It is also integral to the offline identification of electrons and the reconstruction of prompt photons and π°'s for physics analyses.

The Shalshlik ECAL technology can only provide a single position for the incoming showering electromagnetic particles. The resolution on this position is limited by the large fluctuations in the electromagnetic showers development and to the coarse granularity, at best matching one Moliere radius. The transverse positions of photons on the ECAL front face are estimated from the energy-weighted barycenters of the neutral ECAL clusters. This barycenter is corrected for various experimental effects, such as the S-shape, incidence angle, and shower penetration depth [27]. The parameters of the ECAL clusters, barycenter and spread, are also used to select charged (neutral) clusters by (anti)matching of the clusters with reconstructed charged tracks.

As shown in Fig. 20, we obtain a position resolution of 1.4 mm in the innermost region of ECAL for energetic photons from $B_d \to K^* \gamma$ decay. The resolution increases to 6 mm in the outer region which has more coarse granularity. The variation of the resolution with photon energy and with different SPD information is illustrated in Fig. 21.

The SPD, PS and HCAL resolutions are approximately half the pad size due to the fact that the SPD is a binary detector, the small transverse development of the shower in the first radiation lengths for the PS and the large cell size for HCAL, respectively.

6.4 Impact of misalignment

The possible impact of a misalignment of the calorimeter are discussed below.

LHCb Alignment Strategy
LHCb Experiment
6   Calorimeter Alignment

Ref: *LHCb-2006-035*
Issue: *1*
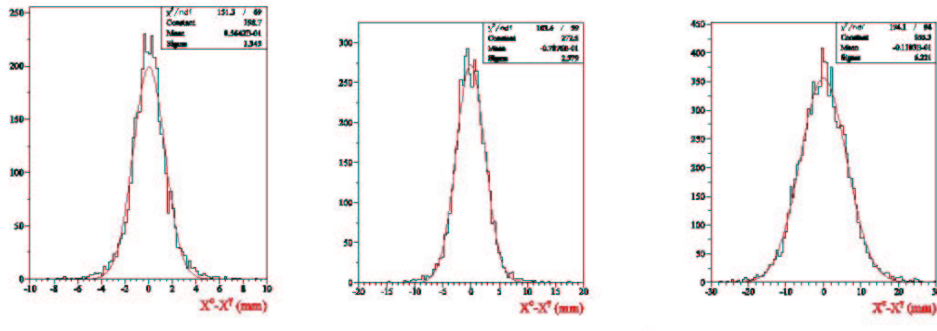**Date:** *June 19, 2006*

Figure 20   Transverse position resolution of the ECAL for energetic photons from the $B_d \to K^* \gamma$ decay. The position is estimated from the energy-weighted barycenter of the ECAL clusters. From left to right : inner, middle and outer ECAL regions.
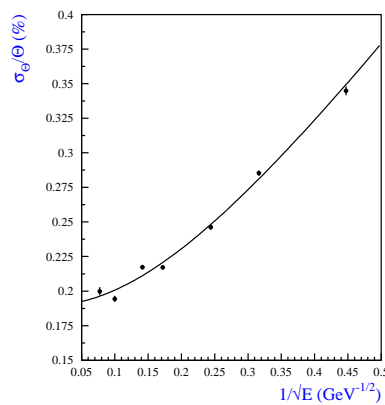

Figure 21   Angular resolution on the photon direction as a function of its energy.
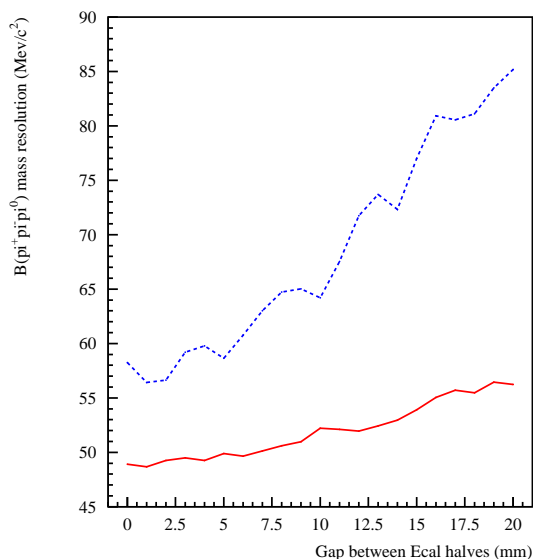
LHCb Alignment Strategy
LHCb Experiment
6 Calorimeter Alignment

Ref: *LHCb-2006-035*
Issue: *1*
Date: *June 19, 2006*

Figure 22 Mass resolution of reconstructed $B \rightarrow \pi^+\pi^-\pi^\circ$ as a function of the half-gap between ECAL halves. The solid red curve indicates the B decays involving a π° reconstructed as a pair of resolved photons. The dashed blue curve correspon ds to B decays involving a π° with merged photon showers leading to a single ECAL cluster and reconstructed according to a dedicated procedure. This latter configuration corresponds to the most energetic π°s

- Photon reconstruction : the incorrect photon momentum assignment resulting from an ECAL misalignment will degrade the mass resolution of reconstructed B decays and of the intermediate resonances involving prompt photons or π° (radiative $B \rightarrow X\gamma$, $B \rightarrow \pi^+\pi^-\pi^\circ$, $B \rightarrow \rho\rho$, $B \rightarrow J\Psi\eta(\pi^+\pi^-\pi^\circ)$, ...). The mass resolution of B decays involving neutrals is however dominated by the ECAL energy resolution and thus these B decays have a limited sensitivity to small mis-alignments.

  As an illustration, Fig. 22 displays the mass resolution of reconstructed $B \rightarrow \pi^+\pi^-\pi^\circ$ candidates as a function of the misalignment of the ECAL halves. As can be seen in the case of the most energetic π°, a 1 cm displacement of both the ECAL halves (well above the expected 1 mm precision on the ECAL halves closing) leads to a limited degradation of the mass resolution at the 10% level.

  Concerning lower mass resonances, the mass resolution of the purely neutral π° decay is to a first approximation unaffected by a global misalignment of the calorimeter structure. Such misalignment could however have a larger relative effect on $\eta \rightarrow \pi^+\pi^-\pi^\circ$ or $\eta' \rightarrow \rho\gamma$ resolution. In addition, it could have some sizable impact on the performance of the selections via the mass window cuts that are applied.

  The mis-reconstruction of photon momenta could also affect the proper time measurement of the B decay. A correct proper time measurement is an important issue for the time-dependent asymmetry measurement of B decay and in particular for the analysis of the $B_s \rightarrow D_s\rho$ decay, aimed at providing a measurement of Δm_s. Figure 23 displays the systematic shift on the proper time reconstruction for the $B \rightarrow \pi^+\pi^-\pi^\circ$ decay as a function of the ECAL halves misalignment. The typical resolution on the proper time for such a decay is of order of $\sim$40 fs. A 2 femto-seconds systematic shift of the proper time measurement is observed for a large 1 cm lateral misalignment of both ECAL halves, which is about ten times larger than expected based on the hardware alignment alone.

- Electron identification : the calorimeter system provides the main discrimination for electron
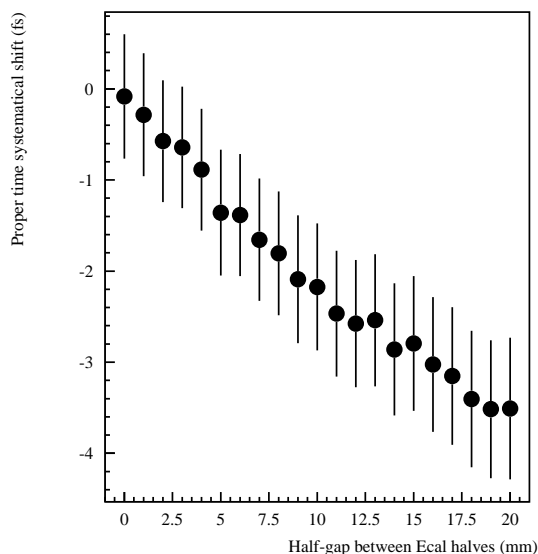
LHCb Alignment Strategy
LHCb Experiment
6   Calorimeter Alignment

Ref: *LHCb-2006-035*
Issue: *1*
Date: *June 19, 2006*

Figure 23 Systematic shift (fs) on the the reconstructed $B \to \pi^+\pi^-\pi^\circ$ proper time as a function of the half-gap between ECAL halves.

identification. Electron identification (ID) is of major importance for the $J/\Psi \to ee$ reconstruction but also contributes to the performance of B flavor tagging via the identification of semi-leptonic B decays.

The position measured in the calorimeter system is used at many places for the purpose of electron ID. First, the main electron ID estimator is a χ^2 based on the energy-position matching of ECAL clusters with an associated charged tracks. In addition, the procedure for Bremsstrahlung recovery also uses a 2D geometrical matching of the ECAL clusters with the linear extrapolation of the electron tracks before the magnet bending. Energy depositions in the PS and HCAL along the path of an extrapolated charged track are also used to aid in rejecting charged hadron background.

These pieces of information are combined to form a Delta-Log-Likelihood for electron ID.

The identification procedure has minimal sensitivity to small misalignments due to the large transverse spread of the electromagnetic shower. However, the impact on electron ID and B-tagging performance has to be quantified with a more detailed study.

- A large relative SPD/PS/ECAL mis-alignment could affect the Level-0 trigger efficiency. For mis-alignments smaller than the half PS/SPD cell size, the impact on the trigger is negligible since the Level-0 electron (photon) candidates are identified by the coincidence of a PS and (no) SPD hits in front of a 2×2 cells ECAL cluster.

6.5   Alignment strategy and software issue

Due to the limited position resolution of the detector the precise positioning already achieved during the ECAL and the HCAL installation, the alignment is not likely to be a critical issue for the calorimeter system.

This statement, however, needs to be confirmed with dedicated studies of various final states of interest. Monte-Carlo simulations produced with various misalignments of the calorimeter system will be studied to check the sensitivity.

If required, a procedure for an automated alignment using data will also be developed. The details of the strategy are still to be defined and require a dedicated study. Such a procedure could be based on the measurement of a systematic shift of the track-cluster matching using a large sample

LHCb Alignment Strategy
LHCb Experiment
6 Calorimeter Alignment

Ref: *LHCb-2006-035*
Issue: *1*
Date: *June 19, 2006*

of tracked electrons over the ECAL surface. Geometer fiducial marks will be accessible for hardware re-measurement if a strong misalignment is suspected.

As of this moment, there is no mechanism for handling misalignments in the calorimeter software. Formally, about 100 parameters are needed to describe any translations and rotations of the 'monolithic' calorimeters volumes (calorimeters halves and SPD/PS super-modules). The amount of parameters can be strongly reduced when only considering the relevant displacements : transversal offsets for the calorimeter halves plus the vertical degrees of freedom for SPD/PS super-modules. Such a parametrization has to be implemented in both the simulation and the reconstruction software. For that purpose, the calorimeter description needs to be slightly reorganized in terms of independent calorimeter halves in order to simulate a misaligned architecture. The reconstruction software could easily implement the alignment framework and a means to deal with misalignments.

LHCb Alignment Strategy
LHCb Experiment
7   Muon system alignment

Ref: *LHCb-2006-035*
Issue: *1*
Date: *June 19, 2006*

7   Muon system alignment

7.1   Introduction

The muon system [9] has coarser granularity than the the other tracking stations, and therefore less stringent demands are placed on the alignment. On the other hand, the muon system forms a critical part of the LHCb trigger, and therefore it must be well aligned in order to avoid adverse effects on the trigger. The smallest pads are about 1 cm, so this implies the muon system should be aligned at the level of about 1 mm or better. In this section, we give a brief introduction to the muon system and plans for alignment.

7.2   Muon System Layout

The LHCb Muon System consists of 1368 Multi-Wire Proportional Chambers (MWPC) with anode wire and/or cathode pad readout arranged in 5 stations (M1-M5). Station M1 is located upstream of the Calorimeters system while M2-M5 stations are located downstream. Stations M2-M5 are interleaved by 80 cm thick iron walls to filter out hadrons. Each station is divided into four regions, R1-R4, where R1 is the innermost and R4 is the outermost with respect to the beam-pipe.

The system follows a projective geometry pointing to the interaction point (IP), and therefore the MWPC dimensions in the 5 stations scale (roughly) with the distance from the IP. In addition, in going from region R1 to region R4, the pad dimensions double at each step (*i.e.* pad dimensions in R2 are double with respect to R1 and so on...). There are then 20 different types of MWPCs chambers whose dimensions depends on the position in the detector labeled by station and region (*i.e.* M1R1, M1R2..... M5R4).

7.3   The L0 muon trigger

The Muon detector, in addition to the role that it plays in muon identification, is also part of the L0 trigger, for which it provides a fast P_t measurement with a precision of about 20%. The L0 muon trigger searches for muon tracks with large transverse momentum where a muon track is defined by a set of hits in all five muon stations which form a straight line and point back to the interaction point. The track finding process starts from the hit in station M3 (the seed of the track) and looks for corresponding hits in the other four stations within search windows (referred to as a Field Of Interest (FOI)), centered approximately on the straight line extrapolation to the IP. Once a muon track is found, its transverse momentum P_t is calculated from the position of the hits in M1 and M2, and assuming a single kick from the magnetic field.

Critical regions

Given the layout of the Muon System, made of 1368 separate MWPC chambers, it is clear that the hardware alignment of each single chamber is very important. The alignment becomes rather critical in the innermost regions (R1 and R2) of stations M1-M3, where the pad dimensions are of the order of 1 cm (see Table 7).

Table 7   Dimensions of the pads (cm x cm) for all the 20 zones in the muon detector.

	M1	M2	M3	M4	M5
R1	1.0x2.5	0.63x3.1	0.67x3.4	2.9x3.6	3.1x3.9
R2	2.0x5.0	1.3x6.3	1.4x6.8	5.8x7.3	6.2x7.7
R3	4.0x10.0	2.5x12.5	2.7x13.5	11.6x14.5	12.4x15.5
R4	8.0x20.0	5.0x25.0	5.4x27	23.2x29	24.8x30.9

LHCb Alignment Strategy
LHCb Experiment
7   Muon system alignment

Ref: *LHCb-2006-035*
Issue: *1*
Date: *June 19, 2006*

Table 8 Particle deviations due to multiple scattering in material: angle (θ^{MS} [mrad]) and position (Δt_e [mm]) at each detector plane for a 10 GeV/c muon.

Muon station	Material preceding the detector	θ^{MS} [mrad]	σ^{MS} [mm]
$M1$	RICH2	0.44	0.51
$M2$	ECAL HCAL Preshower	14	24.6
$M3 - M5$	Muon filters	9.7	6.7

Hardware alignment

All the chambers of the muon system will be precisely positioned on their own half-station support panels while they are retracted from their nominal positions, and then moved into the data-taking position. Half stations M2-M5 are on the same support structure and will be moved into their nominal positions together.

The procedure for the positioning of each chamber on its support panel is as follows:

1. Each chamber will be installed on the half station support panel using precisely positioned chamber supports (two for each chamber).

2. The x-y position of the chamber will be measured using a laser distance measurement meter (precision of about 1 mm) with respect to reference points placed on the border of each half station support panel.

3. If necessary, the position will be corrected and then the chamber will be fixed.

Once the half stations are assembled, they will be moved together (M2-M5) to their nominal positions and their relative alignment will be surveyed with respect to external reference points placed on each support panel. A fine positioning of each half-station support panel can also be done, if necessary, with a range of ± 10mm and with a precision of about 1 mm in both x and y directions.

7.4   Software alignment

Software alignment will be performed for each station at the beginning of data taking in late 2007, by using a large statistics muon sample. After any opening-closure of a half-station, a software alignment calibration is also recommended to check the half station positioning.

Due to the large material budget needed to stop hadrons and identify muons, tracks crossing the muon stations will undergo large multiple scattering. Moreover the pad sizes can be as large as 309 mm (y in M5R4). For these reasons a software alignment based on tracks will have an intrinsic limited precision.
To get a rough estimate of the uncertainties due to multiple-scattering at each muon station we use the following equations:

$$\theta_0^{MS} \approx \frac{0.0136}{p} \times \sqrt{x/X_0} \times (1. + 0.038 \times ln(x/X_0)) \tag{6}$$

$$\Delta t_e = \frac{1}{\sqrt{3}} \times \Delta z \times \theta_0^{MS}, \tag{7}$$

where θ_0^{MS} is the particle angle rms, Δt_e the RMS deviation to the extrapolated coordinate t_e (x or y) and p is the particle momentum in GeV/c. In Table 8 we show the estimated uncertainties (RMS) due to multiple scattering in each detector plane for a 10 GeV/c muon assuming that its position and direction at the previous tracking/muon station is measured.

A software alignment based on the residual distributions of tracks crossing all the muon stations will be developed to determine the detector alignment constants. The residual, obtained by comparing at each detector plane the extrapolated and the measured coordinates (t_e and t_m in x or y direction) in

LHCb Alignment Strategy
LHCb Experiment
7   Muon system alignment

Ref: *LHCb-2006-035*
Issue: *1*
Date: *June 19, 2006*

error units, will be distributed around zero mean in case of perfect alignment, or non zero mean in case of misalignment.

$$R = \frac{t_e - t_m}{\sqrt{\sigma_e^2 + \sigma_m^2}} \tag{8}$$

By using *B-field off* runs at the beginning of data taking it will be possible to obtain an initial set of alignment constants. Afterward, the alignment will be checked using *B-field on* data, and if neccesary the alignment parameters will be adjusted.

7.5   Alignment studies strategy

A misalignment of the muon system will have its greatest impact on the L0 trigger, since it can change the on-line Pt measurement and/or muon candidate selection efficiency. The effect on offline reconstruction (particle ID) should be less significant. In order to give a quantitative evaluation of the different effects of a misaligned muon detector on the L0 trigger and muon identification, we plan to simulate several samples with different misalignment scales (from $O(1 \text{ mm})$ to 1 cm) for:

1. the whole muon detector with respect to the rest of LHCb;

2. M1 station with respect to M2-M5;

3. each station;

4. a single chamber in the more critical regions (closer to the beam-pipe in M1 and M2).

Two main studies will be carried out:

1. L0 muon trigger performances as a function of misalignment scale (efficiency to signal, minimum bias retention, P_t bias, charge asymmetry);

2. Muon identification performances (efficiency, pion contamination);

To determine and correct for misalignments, a stand-alone tool will be developed which will use muons that cross all the detectors and will match segments in the T-Stations with hits in the muon chambers. The tools to simulate misalignments now exist within the LHCb software framework. To study L0 trigger efficiency a sample of 500,000 minimum bias and 30,000 specific B decay events will be used from the upcoming data challenge. Higher statistics might be necessary to achieve the desired precision.

LHCb Alignment Strategy
LHCb Experiment
8   Absolute Global Coordinates

Ref: *LHCb-2006-035*
Issue: *1*
Date: *June 19, 2006*

8   Absolute Global Coordinates

As discussed in the preceding sections, the LHCb detector if brought into relative alignment by first aligning the tracking system, and then aligning RICH, ECAL, HCAL, and MUON systems to the tracking system. This *relative* alignment is the most critical aspect of the LHCb alignment. However, we ultimately would like to connect these relative positions to an absolute, and unchanging coordinate system. The global coordinate system was introduced in the introduction, and ideally, we would like to express hit coordinates in this global reference frame. As the VELO is the most precise position-measuring device in LHCb, we would naturally expect it to play a central role in the definition of the LHCb global coordinate system. However, the absolute position of the VELO is only known to about 10 μm from the readback of the motion controller, and therefore, this sets a lower limit on our knowledge of the absolute position of the LHCb detector in the LHCb cavern.

Here, we propose to fix the absolute global origin as follows. We simply define x=0, $y = 0$ as the nominal distance of the VELO halves with respect to the (transverse) position of the center of the interaction region (IR). We may choose to define z=0 as the position of one of the VELO sensors. In LHCb, this is about 3 cm. When colliding beams are established in LHCb, we center the VELO halves on the interaction point. The total distance moved my the stepper motor of the VELO is recorded. This offset is one of the several transformations which need to be applied to translate from a local hit coordinate in the local frame of the sensor *i.e.,* r and ϕ, to an absolute global coordinate in the LHCb reference frame (generally x and y). The other coordinate transformations are determined from the internal alignment of the VELO and the alignment of the two halves with respect to one another as discussed in Section 2.

We use the readback of the VELO motion controller to indicate the distance moved by the VELO sensors with respect to the fully retracted position of the VELO. Thus, by monitoring and recording the readback value from the VELO motion controller, we obtain a history of the position the interaction region with respect to our predefined x=0, $y = 0$, $z = 0$. In principle, since only the VELO is moving in between fills, only the VELO's alignment constants need to be updated. As long as the other subdetectors do not move, their alignment parameters should not need to be updated. In practice though, as discussed in the Introduction, RICH1, TT and the T-Stations are in the fringe field of the dipole magnet, and small displacements could be envisaged. Therefore, we will need to run a program that checks their internal alignments as well as their alignment with respect to the VELO. Of course, any change in the T-Station alignment could also affect RICH1 and RICH2 (and ECAL, HCAL and MUON, but they have more coarse resolution), and therefore an automated alignment program for RICH1 and RICH2 will need to monitor and update alignment constants associated with the RICH detectors, if necessary.

The readback of the VELO motion controller is only precise to about 10 μm, and therefore, we only know the absolute position of the VELO to this accuracy. The intrinsic hit resolutions of the TT and the T-Stations are significantly worse than this, and therefore this overall uncertainty should not result in any significant performance in tracking or in the trigger. This 10 μm uncertainty also sets a lower limit on how well we can track changes in the position of the interaction region. In terms of physical measurements, an overall global transformation has no impact on the physics, provided the detector is aligned internally as a whole.

To summarize, we will need to define a convention which establishes the zero of the global coordinate system. For example, we can define $x = 0$ as corresponding to a 3 cm travel of the motion controller. We are also planning on storing the motion controller readback value, and this will be one of the several transformations applied to obtain absolute hit positions in the VELO. Other subdetectors should not include this offset in their local-to-global transformations, since in principle they are not moving with each fill. Alignment processes will need to run during data taking in order to monitor the alignment of each of the subdetectors.

LHCb Alignment Strategy
LHCb Experiment
9   Storage and Retrieval of Alignment Constants

Ref: *LHCb-2006-035*
Issue: *1*
Date: *June 19, 2006*

9   Storage and Retrieval of Alignment Constants

9.1   Introduction

The LHCb Conditions Database (CondDB) [29] project aims to provide the necessary tools to handle non-event time-varying data, including alignment constants. The LHC Computing Grid (LCG) project, *Conditions Objects for the LHC* (COOL, for short) [30], provides a generic Application Programming Interface (API) to handle this type of data and an interface to it has been integrated into the Gaudi framework of LHCb. The interface is based on the Persistency Service infrastructure of Gaudi, allowing the user to load it at run-time only if needed.

Since condition data are varying with time as the events are processed, condition objects in memory must be kept synchronized to the values in the database for the current event time. A specialized service (the Update Manager) has been developed independently of the COOL API to provide an automated and optimized update of the condition objects in memory.

For reconstruction and analysis tasks, a reference copy of the CondDB (the Master Copy) will be duplicated over the LHC Grid. This Oracle database is of critical importance and the addition of new conditions will be limited to a small number of administrators. The only exception to this rule concerns condition data produced online by the alignment algorithms running on the event filter farm.

9.2   Off-line Usage

Alignment constant retrieval from the CondDB is handled automatically via the LHCb Geometry Framework. It insures that the positions of the detector elements used to process an event are valid.

The update of the CondDB is a more complex issue. From the standard user point of view, it is not possible to write anything to the Master Copy of the CondDB. However, more advanced users can use their own local copy of the CondDB and modify it at will. This can be done either through the CondDB Access Service, which is part of the LHCb software, or via Python scripts using directly the COOL interface.

The editing of the Master Copy will be devoted to a small group of super-users who will be in charge of integrating condition values cross-checked by experts. The submission process for Master Copy updates is not formalised yet.

9.3   On-line Usage

During data taking periods, we will have 4000 concurrent processes running in the pit that need to access condition data, mainly at initialization time. A database server will not be able to handle this load, so we plan to publish condition data to the on-line processes in a different way. When the on-line processes have to be initialized, a dedicated process will read the data from the condition database and will send them to a service in each on-line process that will fill the cache of the CondDB access service and notify the update manager service about the values inserted.

Alignment constants produced in the pit, *e.g. from Velo motion controller and alignment algorithms*, will be sent to a dedicated process that will write them to the CondDB. Some of these condition data need to be published to the on-line processes while they are running (e.g. motion controller data used by the alignment algorithms). In this case, the DB writer process will also send the data to the on-line process in much the same way as it happens during the initialization phase. A time delay will be added to the interval of validity of the condition data, when written to the CondDB and when used by the on-line processes. This delay should be greater than the time it takes to propagate the new condition to the cache of all the nodes of the event filter farm. This will ensure that offline processes will be able to use exactly the conditions used online for event processing.

LHCb Alignment Strategy
LHCb Experiment
9   Storage and Retrieval of Alignment Constants

Ref: *LHCb-2006-035*
Issue: *1*
Date: *June 19, 2006*

9.4 Summary

We have described in this document the status and plans for aligning the LHCb spectrometer. For the internal alignment of the tracking system, we expect to use Millepede. Its application to the VELO is mature, and is shown to be unbiased in extracting the critical misalignments. We also expect to use Millepede for the T-Station alignment, and initial indications using a toy Monte Carlo simulation are encouraging. The relative alignment of the VELO and T-Stations will be perfomed by comparing segments at the center of the magnet. The method is simple and robust. Once the VELO and T-Stations are brought into relative alignment, the Trigger Tracker will be aligned by using residuals of TT hits to tracks reconstructed with VELO and T-Station hits. Once the tracking system is aligned we proceed to align the RICH. The HPD array is first aligned using a separate calibration system (design still being finalized). The two-mirror system is then aligned by comparing the reconstructed photon positions with the expected positions (based on the charged tracks' parameters) while allowing for both x and y tilts of each mirror segment. The ECAL will likely be aligned by selecting a clean electron sample and requiring that reconstructed showers match the extrapolated position of the charged track. Lastly, fine alignment of the MUON system will be performed by minimizing the residuals between extrapolate muon candidate tracks and hits in the MUON stations. The LHCb detector geometry and time-dependent conditions are described using XML and the tools for reading and writing to the Conditions Database are mostly in place. We expect to have all aspects of the LHCb alignment in place for the upcoming *Alignment Challenge and Detector Commissioning* in the Fall of 2006.

LHCb Alignment Strategy
LHCb Experiment
10 References

Ref: *LHCb-2006-035*
Issue: *1*
Date: *June 19, 2006*

10   References

[1] LHCb Reoptimized Detector Design and Performance, CERN/LHCC 2003-030 (Sept. 9, 2003)

[2] LHCb VELO Technical Design Report, CERN-LHCC-2001-011.

[3] J. Gassner, M. Needham, and O. Steinkam, LHCb Internal Note, LHCb-2003-140 (2003); J. Gassner, F. Lehner, and S. Steiner, LHCb Internal Note LHCb-2004-110 (2004).

[4] LHCb Inner Tracker Technical Design Report, CERN-LHCC-2002-029.

[5] LHCb Outer Tracker Technical Design Report, CERN-LHCC-2001-024.

[6] LHCb Magnet Technical Design Report, CERN-LHCC-2000-007.

[7] LHCb RICH Technical Design Report, CERN-LHCC-2000-037.

[8] LHCb Calorimeters Technical Design Report, CERN-LHCC-2000-036.

[9] LHCb Muon System Technical Design Report, CERN-LHCC-2001-010.

[10] LHCb Trigger System Technical Design Report, CERN-LHCC-2003-031.

[11] Privite communication with: Andrej Gorisek, HERA-b; Daniele Pedrini, FOCUS; Craig Dukes, HyperCP; Charles Newsome, SELEX; Keith Thorne, E791; and personal experience from E706.

[12] F. Teubert, *B-Field Map*, LHCb Week Talk, March 9, 2006, http://indico.cern.ch/conferenceDisplay.py?confId=1130.

[13] R. Lindner, *Definition of the LHCb Coordinate System*, EDMS Note 372642.

[14] S. Viret, C. Parkes & D. Petrie - *LHCb VELO software alignment. Part I: the alignment of the VELO modules in their half boxes*, LHCb 2005-101.

[15] V. Blobel and C. Kleinwort, *A new method for the high-precision alignment of track detectors*, hep-ex/0208021; V. Blobel, *A new method for the high-precision alignment of track detectors*, CONFERENCE ON ADVANCED STATISTICAL TECHNIQUES IN PARTICLE PHYSICS Conference Contribution, **18-22 March 2002** (Durham, UK); V. Blobel, *Software Alignment for Tracking Detectors* DESY SEMINAR: COMPUTING IN HIGH ENERGY PHYSICS, [http://www.desy.de/ blobel/atalk.pdf]; V. Blobel, *Software Alignment for Tracking Detectors*, WORKSHOP ON TRACKING IN HIGH MULTIPLICITY ENVIROMENTS, [http://ckm.physik.unizh.ch/time05].

[16] J. Palacios - *LHCb Geometry Framework*, https://uimon.cern.ch/twiki/bin/view/LHCb/GeometryFramework.

[17] A. Froton, J.N. Joux and J-Ch. Gayde, *LHCb - Outer Tracker Bridge and Tables Geometric control in Van Halteren Metaal B.V. factory, Bunschoten - Netherlands*, EDMS NO: 716870.

[18] Antonio Pellegrino and Henk Schuijlenberg, *Supply of Support Structure for the LHCb Outer Tracker - Lower Part*, EDMS NO: 696884.

[19] Antonio Pellegrino and Henk Schuijlenberg, *Supply of Support Structure for the LHCb Outer Tracker - Upper Part*, EDMS NO: 701347.

[20] S. Bachmann and A. Pellegrino, *Geometry of the LHCb Outer Tracker (Part I)*, Internal Note: LHCb-2003-035.

[21] M. Bräuer, *Alignment des HERA-B Vertexdetektors*, MPI Heidelberg, Ph.D Thesis, 2001.

[22] M. Needham, O. Steinkamp, U. Straumann and A. Vollhard, "Raw data format and readout partitioning for the Silicon Tracker," Internal Note:LHCb-2004-044

[23] A. Gorišek et al, Nucl. Instr. and Meth. **A 433** (1999) 408.

[24] A. Papanestis, *Limits of software compensation for mirror misalignment of the RICH detectors*, LHCb note **2001-141 RICH**.

LHCb Alignment Strategy
LHCb Experiment
10   References

Ref: *LHCb-2006-035*
Issue: *1*
Date: *June 19, 2006*

[25] http://www.cern.ch/minuit.

[26] G. Aglieri Rinella et al, *Characterisation and compensation of magnetic distortions for the pixel Hybrid Photon Detectors of the LHCb RICH*, Nucl. Instr. and Meth. **A 553** (2005) 120.

[27] O. Deschamps *et al*, *Photon and neutral pion reconstruction*, LHCb-2003-091.

[28] EDMS Notes 640197, 579149, 584037, 584040, 607907.

[29] M. Clemencic, Nicolas Gilardi, and J. Palacios, *The LHCb Conditions Database Framework*, Conference on Computing in High Energy Physics (CHEP06), Mumbai, India, Feb. 13-17, 2006; More information can be found at the project web page at: http://lhcb-comp.web.cern.ch/lhcb-comp/Frameworks/DetCond/.

[30] Andrea Valassi, *COOL Development and Deployment, Status and Plans*, Conference on Computing in High Energy Physics (CHEP06), Mumbai, India, Feb. 13-17, 2006; COOL Project Web Page: http://lcgapp.cern.ch/project/CondDB/.